LEVEL II

(12)

AD A080210

DDC
FEB 4 1980
E

DDC FILE COPY

This document has been approved for public release and sale; its distribution is unlimited.

(12)

Technical Report No. 2
Office of Naval Research
Contract No. N00014-76-C-0808

See 1473

DDC
RECEIVED
FEB 4 1980
E

ANALYTICAL MODELLING OF STRUCTURAL DISTORTION IN SHIP STRUCTURES PRODUCED BY WELDING

by
P. J. Cacciatore
and
R. Morante

~~Systems Technology Department~~
Electric Boat Division
GENERAL DYNAMICS
Groton, Connecticut

Dec., 1979

Production in whole or in part is permitted for any purpose of the United States Government.

Prepared for
Office of Naval Research
Metallurgy Program
Arlington, Virginia 22217

This document has been approved for public release and sale; its distribution is unlimited.

U443-79-087

TABLE OF CONTENTS

		Page
I.	BACKGROUND AND OBJECTIVES	1
II.	EXPERIMENTAL RESULTS - UNRESTRAINED PLATE	5
	A) Test Set-up	5
	B) Distortion Data Analysis	5
III.	MATERIAL PROPERTY DESCRIPTION	15
	A) Introduction	15
	B) Properties of HTS Steel	17
	C) Idealization of Material Properties	21
IV.	APPLICATION OF THE SHRINKAGE FORCE METHOD (SFM) TO WELDING UNRESTRAINED PLATE	25
	A) Introduction	25
	B) Analytical Approach	27
	C) Mathematical Models	29
	D) Discussion of Results	32
V.	APPLICATION OF THERMOPLASTIC ANALYSIS TO WELDING UNRESTRAINED PLATES	57
	A) Introduction	57
	B) Analysis Methods	61
	C) Analysis Results	64
VI.	CONCLUSIONS AND RECOMMENDATIONS	78
	A) Shrinkage Force Analysis	78
	B) NONSAP Analysis	81
	C) Recommendations	84
VII.	REFERENCES	86

Accession For
NTIS GRA&I
DDC TAB
Unannounced
Justification
By
Distribution/
Availability Codes
Dist | Avail and/or special
A

I. BACKGROUND AND OBJECTIVES

In July 1976, a contract was awarded by the Office of Naval Research to Electric Boat Division in the area of computer analysis of welded ship structures. The overall objective of this research was to apply and further develop where necessary the technology for predicting distortion of submarine structure due to welding. The underlying motivation in providing this technology is that it can be used in design and construction of submarines to help determine the most cost effective weld joint designs and welding procedures. The specific objectives of the initial contract were;

1) implementation of MIT finite element computer programs for prediction of temperatures, residual stresses, and distortion due to welding,

2) evaluation of MIT computer programs on a fusion weld of two plates and comparison with results obtained by MARC-CDC finite element program (1)*,

3) analysis of a butt welded unrestrained plate with MIT computer codes and comparison with test results.

*Numbers in parenthesis indicate references.

The results of that study are documented in Reference 2. In June 1977, a contract modification extended the scope of the current contract to the following major technical objectives:

1) transient thermoplastic analysis of a butt welded unrestrained plate using the Electric Boat Division (EBDiv.) modified NONSAP finite element computer code,

2) further development and application of EBDiv. Shrinkage Force Method (SFM) to welding analysis including investigation of weld bead sequencing, non-symmetry in the weld groove and remelt effects. The SFM is a simplified analytical approach for predicting weld distortion. The method is described in Section IV-A of the report.

The results of this study are documented in this report.

The technical objectives for the modified contract were developed on the basis of the results of the first year's work and discussions with cognizant ONR and MIT technical personnel.

Several problem areas in the use of the MIT computer programs for welding simulation were uncovered during the first year. As a result of these problems, EBDiv. began modification of its own in-house software for analyzing weld problems. This resulted in the implementation of two computer codes. The first code, TEMP (2), performs the nonlinear heat transfer of two dimensional solids. TEMP was used in the first year of the contract to calculate the transient temperature solutions for the butt welded unrestrained plate problem. The second code, NONSAP (2), was modified to handle two dimensional thermo-plasticity problems with temperature dependent material properties.

The first objective of the modified contract was to study the distortion and stresses resulting from the butt welding of the unrestrained plate using the modified NONSAP program. The transient temperature solutions from the TEMP program would be used as the driving thermal gradients for the problem.

It became apparent in the early stages of this study that the high level of technology available in the more sophisticated computer programs for welding simulation would be costly to employ on many shipyard problems. This is particularly true if parametric studies involving several variables were required. This degree of sophistication would be needed for detailed

analyses, such as residual stresses and fracture of weldments. However, many shipyard problems stem from the geometric distortions caused by welding; in many cases design and/or fabrication decisions can be made on the basis of relative distortion comparisons through parametric study.

In light of these current requirements, a second objective, the study and application of approximate "weld simulation" methods, was established. In particular the Shrinkage Force Method (SFM) has been extended to two dimensional solids. The method is employed in the GENSAM (3) computer program and studies concerning weld sequencing, weld symmetry, and remelt have been performed under the modified contract. Electric Boat has concurrent with this contract, initiated an IRAD (4) (Internal Research and Development) task which emphasizes the employment of approximate "weld simulation" techniques such as SFM in shell welding. Under this task, the weld problem is being viewed as a layered shell analysis in the weld region, with the layers having the material and thermal characteristics of the weld deposit. The analytical approach utilizes a finite difference shell model as opposed to the two dimensional solid finite element method which is currently employed in the (R studies.

II. EXPERIMENTAL RESULTS - UNRESTRAINED PLATES*

II-A. Test Set-up

Figures II-1 and II-2 contain plan and elevation views of the test set-up along with a detail of the weld groove geometry.

A total of 15 weld beads, 3 initial root passes by shielded metal arc and 12 fill passes by submerged arc were made. Figure IV-3 contains a macro section of the final welded region. Bead number one was removed by backgrinding.

Distortion data was collected via dial indicators, potentiometer transducers and strain gage beam instruments. Their relative locations are given in Figure II-3.

II-B. Distortion Data Analysis

Figures II-4A and 4B contain the measured deflections at each of the gauge locations for welding of the first side. There is a significant discrepancy between the readings from the transducer labelled B and the five other gauges. Being unable to account for the discrepancy, it was decided that the gauge B data would not be used in the evaluation of experimental results.

*This test was performed under a 1975 EBDiv. IRAD project (Ref. 5).

Figure II-5 shows the average deflections of gauges A and D, C and F as compared with the transducer at E. The early bead distortion response at E is greater than the average of the responses at the ends of plate. This indicates a slight bowing upward which reverses to downward at about bead 7. Overall, Figure II-5 shows a nearly uniform deflection pattern along the length.

Figure II-6 contains the plots of changes of deflections for each bead. The data indicate that the largest changes occur in going from bead 1 to bead 3, with the second largest increment occurring in the deposit of bead 5.

Figure II-7 contains plots of tip deflections and rotation at E along with their associated increments. The data in Figure II-7 was used as the basis for comparison with analytical results.

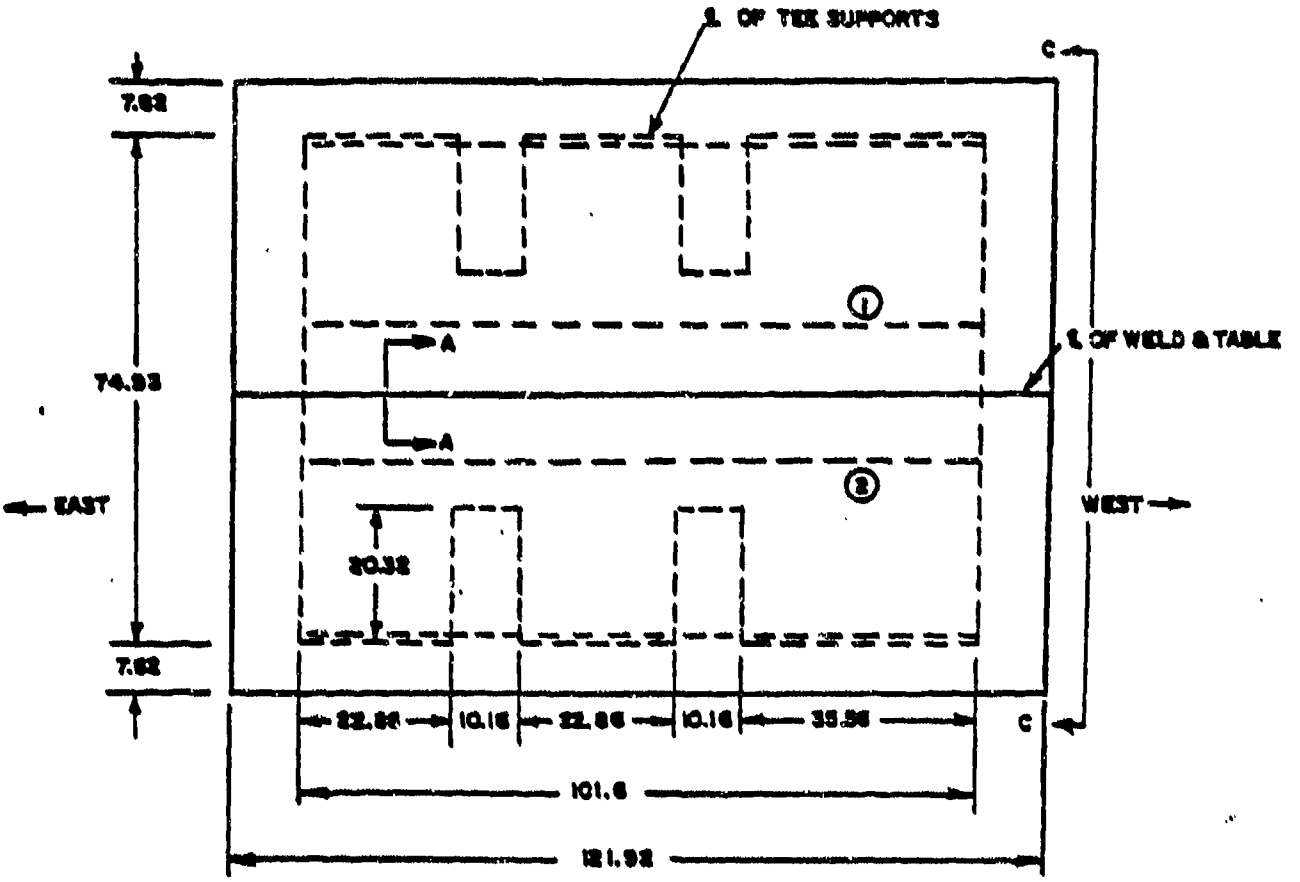

PHANTOM LINES
TABLE OUTLINE

SOLID LINES TEST PIECES
TO BE WELDED 1 & 2

DIMENSIONS IN CENTIMETERS
MATERIAL HT'S

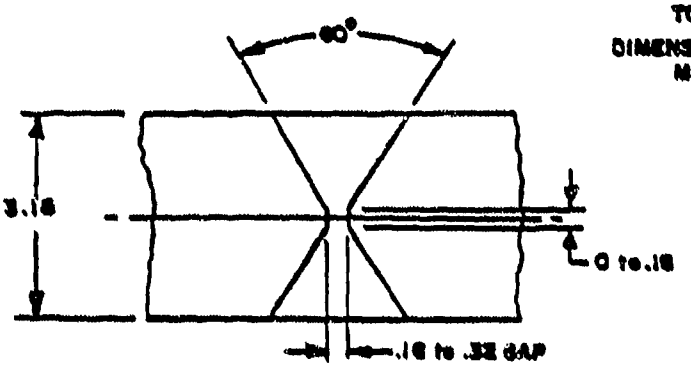

SECTION A-A
WELD JOINT DETAIL
DOUBLE V BUTT JOINT
FULL SCALE

PLAN VIEW OF TEST SET-UP

FIGURE II-1

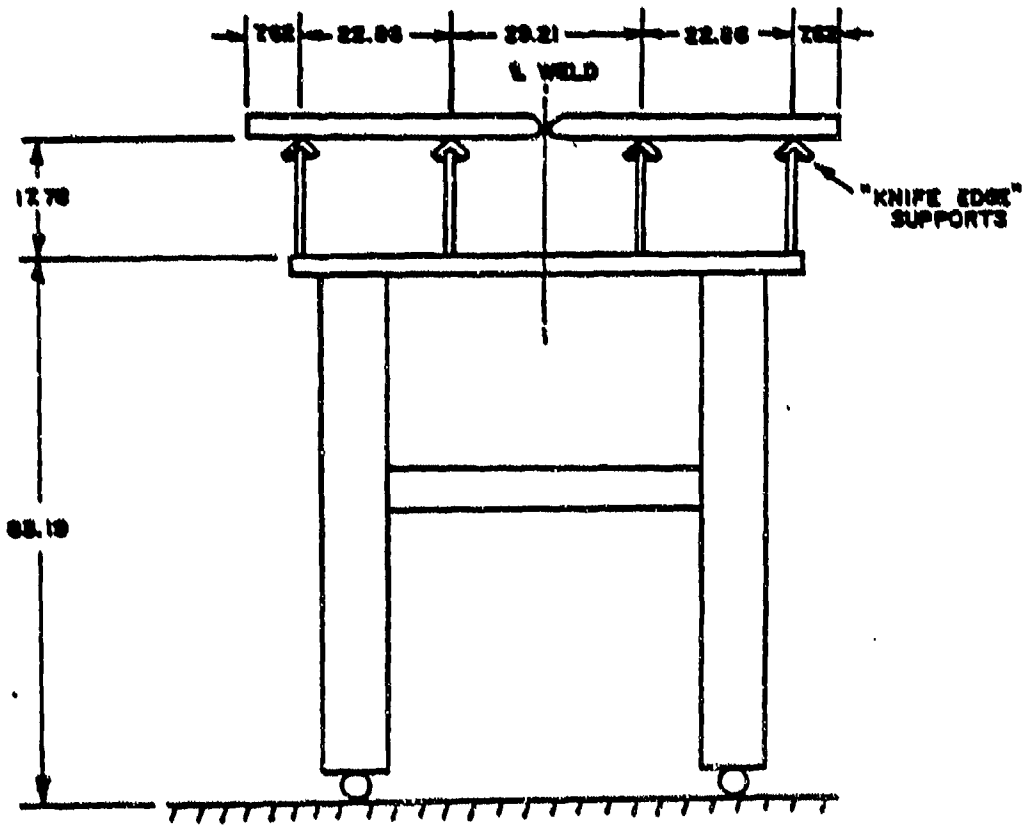

DIMENSIONS IN CENTIMETERS

ELEVATION-VIEW at SECTION C-C OF TEST SETUP
FIGURE II-2

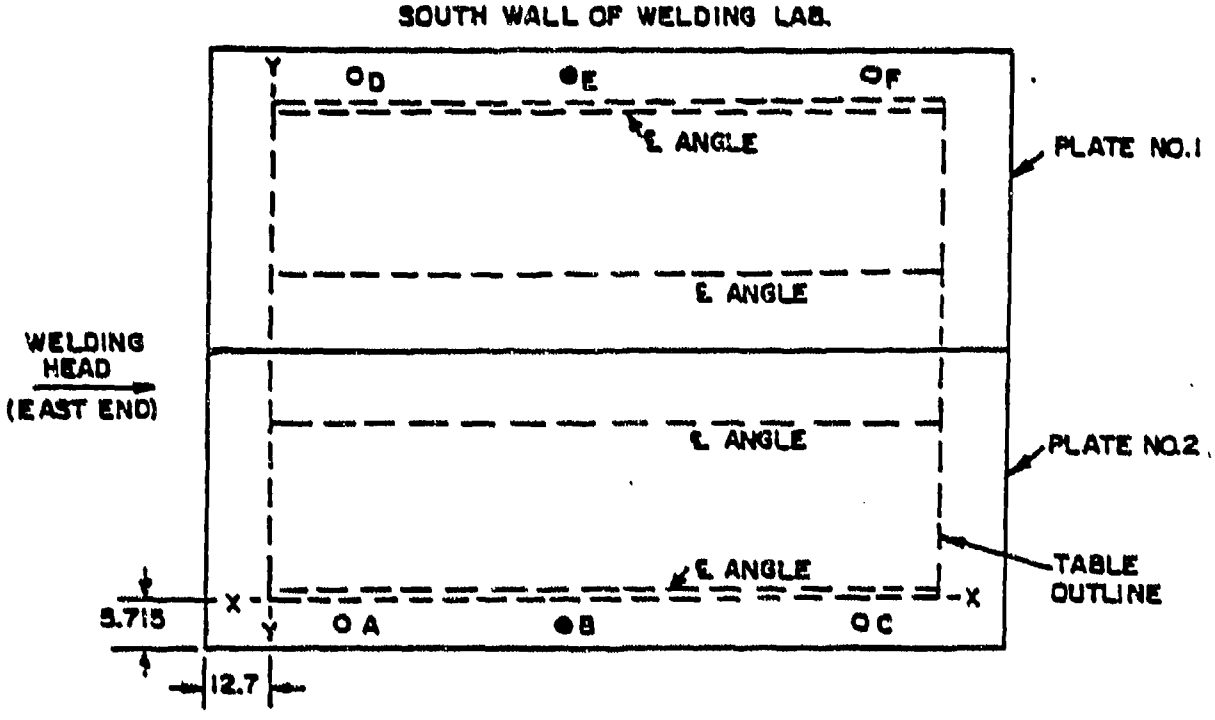

DISPLACEMENT MEASUREMENT DEVICES	GAGE NO	"X"	CM.	"Y"	CM
	1A	4 1/2"	11.43	-1 7/8"	-4.76
O DIAL INDICATOR	2B	20 1/4"	51.44	-1 7/8"	-4.76
	3C	35 1/2"	90.17	-1 7/8"	-4.76
● POTENTIOMETRIC TRANSDUCER	10D	4 1/2"	11.42	31 7/8"	80.96
	11E	20 1/2"	51.44	31 7/8"	80.96
	12F	35 1/2"	90.17	31 7/8"	80.96

LOCATIONS FOR DEFLECTION MEASUREMENTS
(OUT OF PLANE)
FIGURE II-3

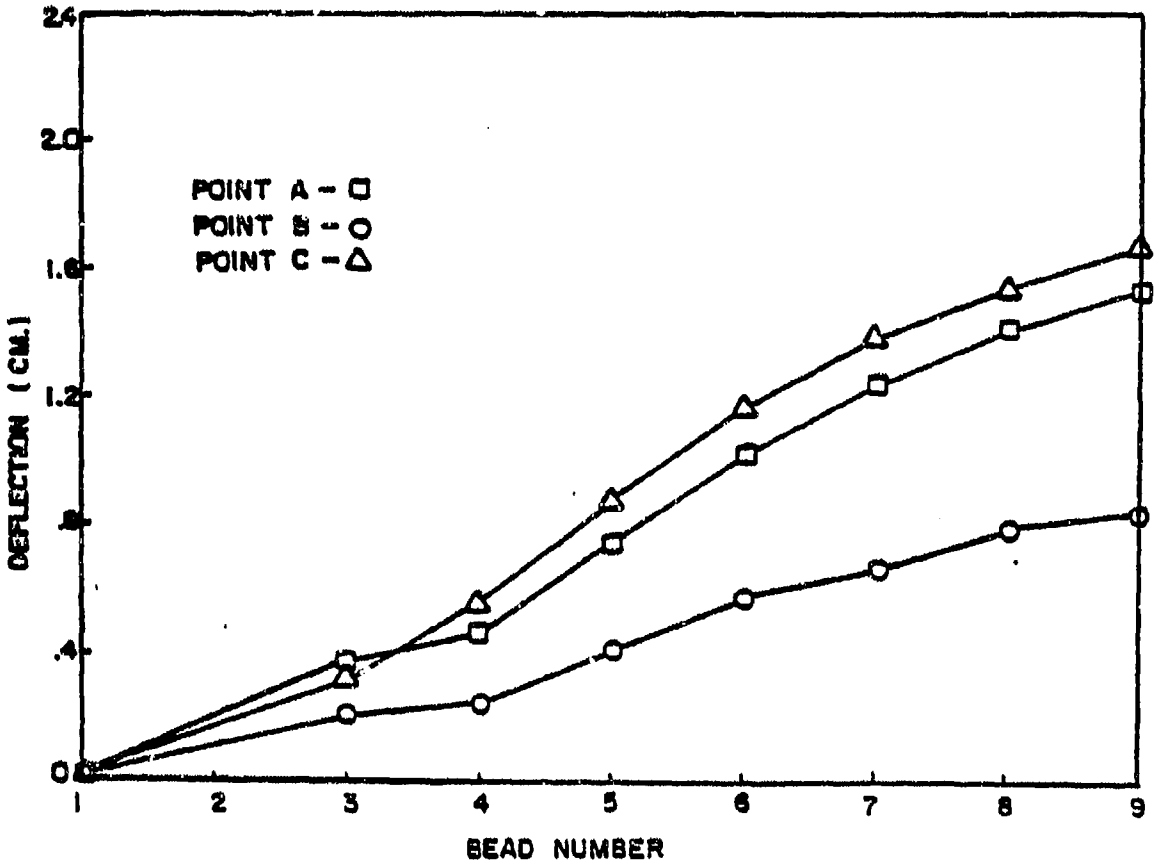

MEASURED CUMULATIVE PLATE DEFLECTION vs BEAD NUMBER

FIGURE II-4A

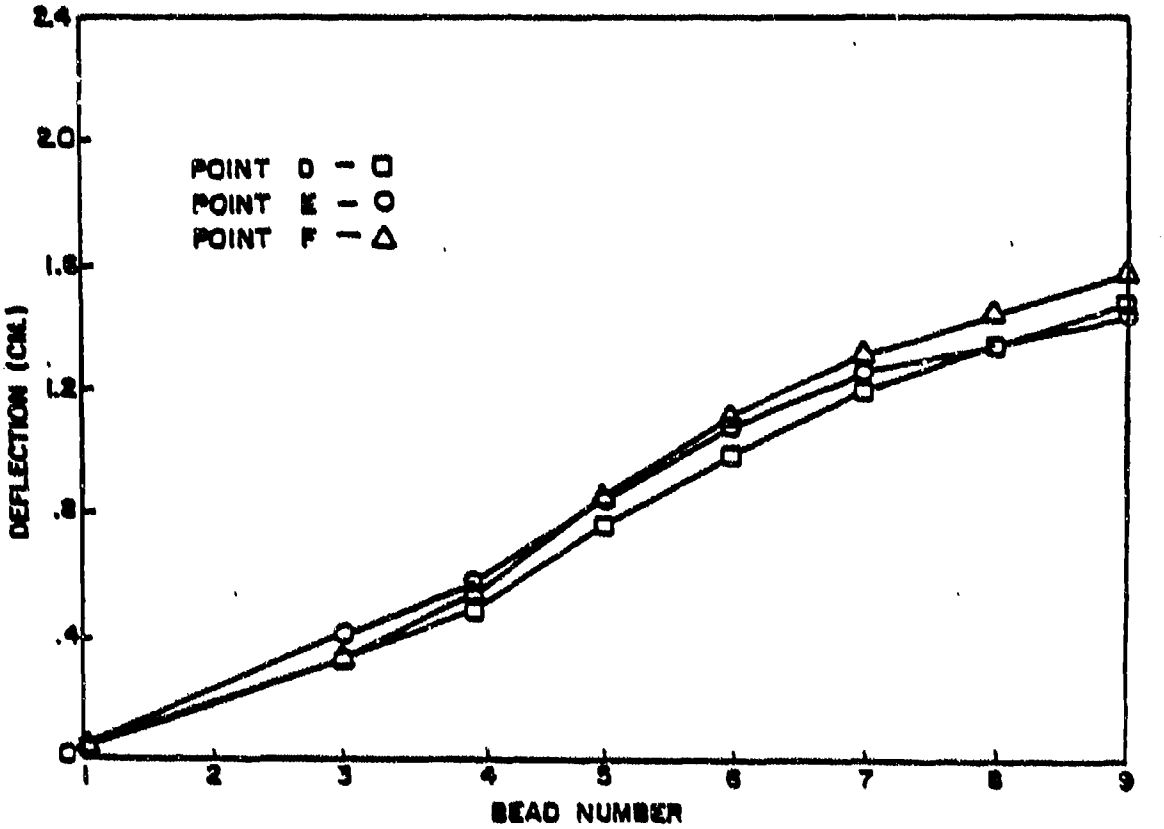

MEASURED CUMULATIVE PLATE DEFLECTION vs BEAD NUMBER

FIGURE II - 4B

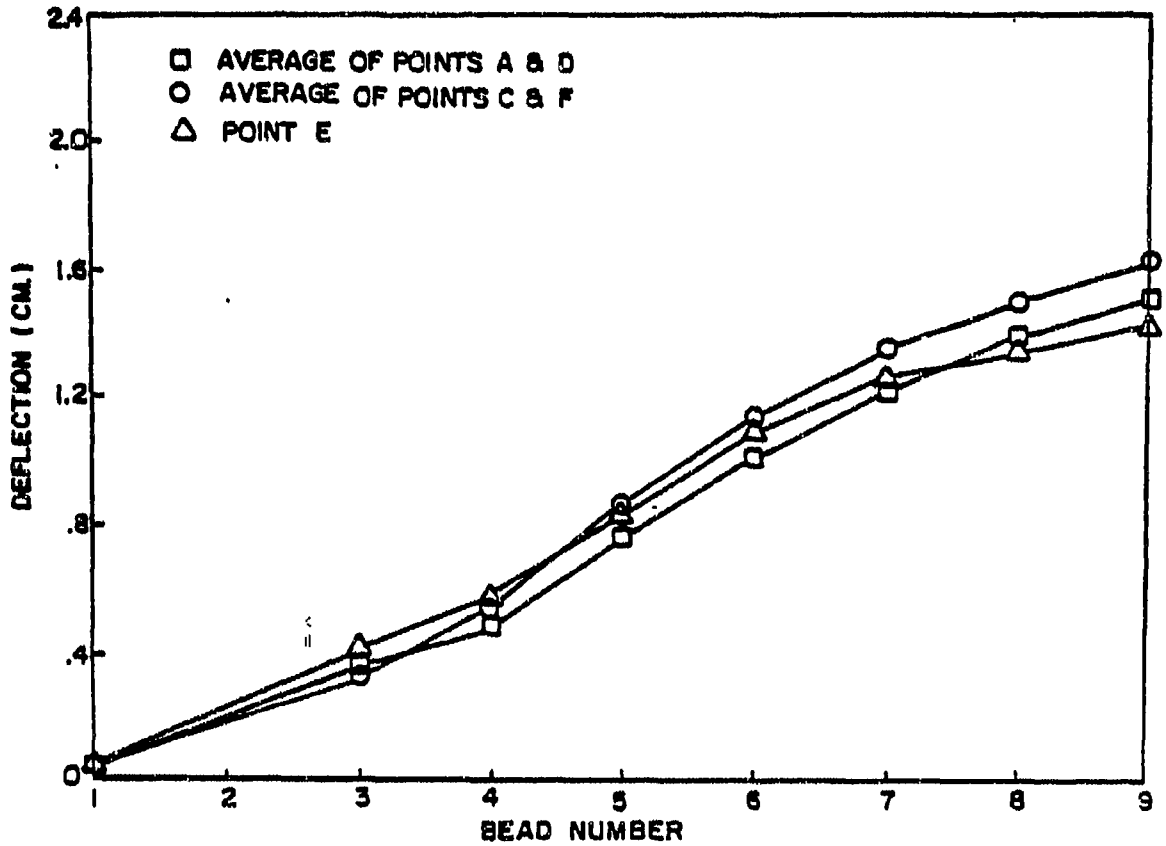

AVERAGE OF MEASURED END DEFLECTIONS vs BEAD NUMBER
(CUMULATIVE)

FIGURE II-5

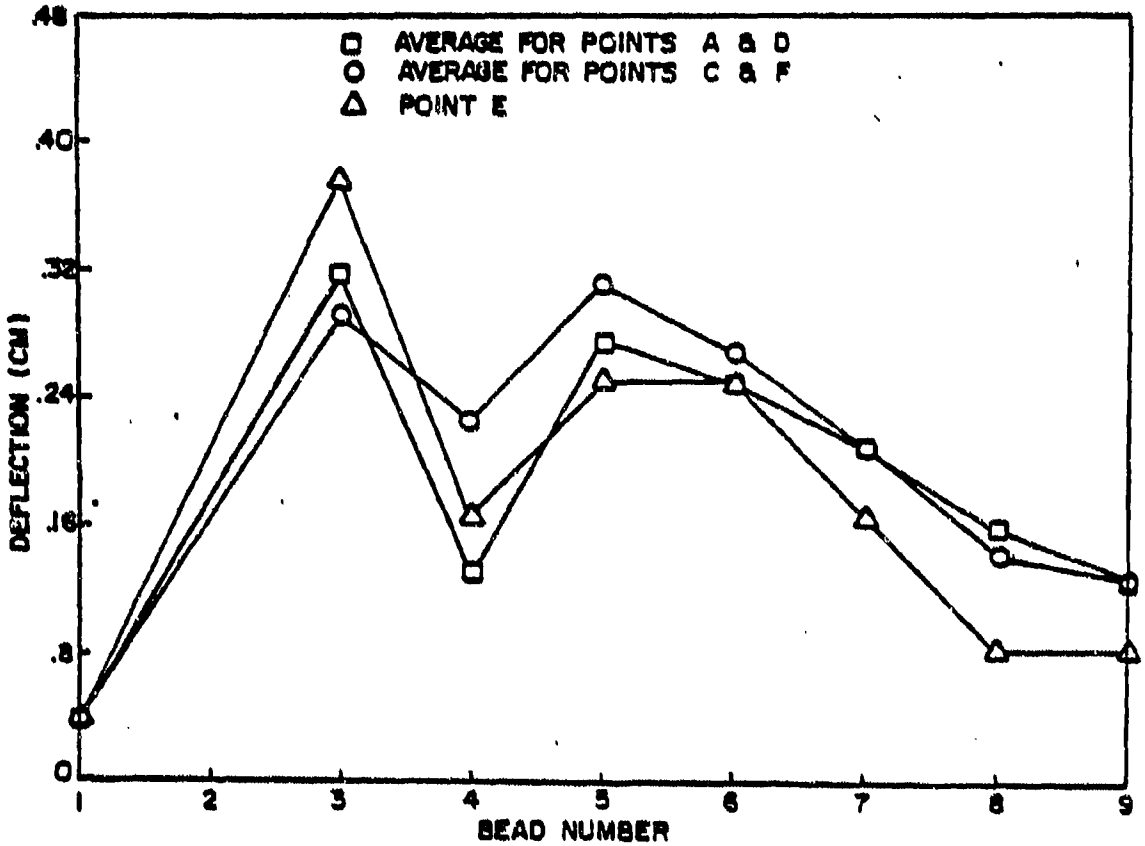

MEASURED INCREMENTAL DEFLECTIONS FOR EACH BEAD

FIGURE II-6

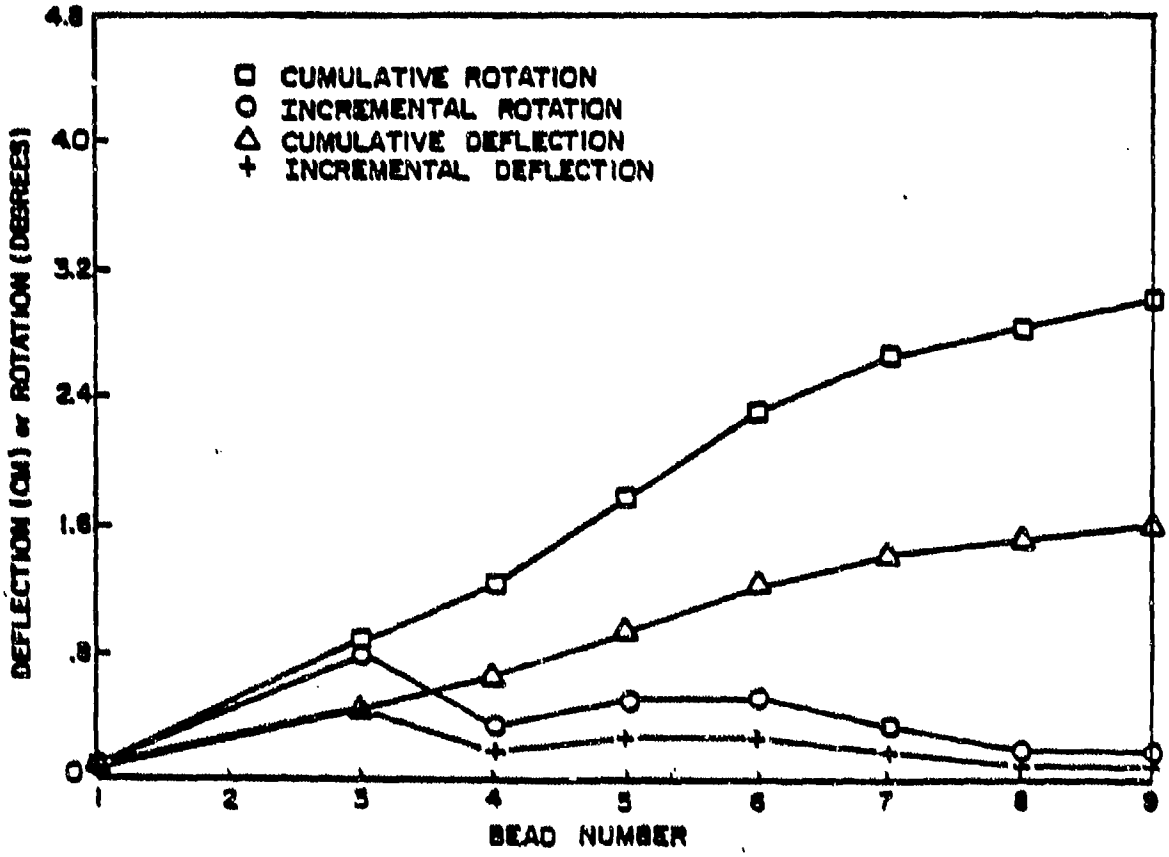

CUMULATIVE AND INCREMENTAL TIP DEFLECTION, ROTATION vs BEAD NUMBER (BASED ON MEASUREMENT AT POINT E)

FIGURE II-7

III. MATERIAL PROPERTY DESCRIPTION

III-A. Introduction

One of the most difficult aspects of attempting to analytically characterize the welding process is the definition of material properties over the wide range of temperatures involved. For many existing steels, this definition does not appear to exist. An additional complication occurs when the material properties of interest are sensitive to both temperature and the rate of cooling (heating). Existing available data is very limited in scope, even for the most recently developed high strength steels.

A successful analytical simulation of welding is directly dependent on an ability to characterize, through a mathematical material model, the behavior of the material in the weld region. This mathematical model is in turn dependent upon properties such as the elastic modulus and coefficient of expansion, etc. which must be experimentally determined. There is a degree of doubt as to the existence of an adequate mathematical material model that would precisely represent the behavior in the weld puddle region.

In this study, the material is characterized in two ways. For the shrinkage force analysis, the material is assumed to be

quasi-linear. The properties take on different discrete values over certain temperature ranges and behavior is assumed to be linear over each temperature range. The NONSAP analysis employs a thermal plasticity model which allows:

a) temperature dependence of Young's Modulus (E), Yield Stress (σ_y), Strain Hardening Modulus (E_T) and Coefficient of Thermal Expansion (α_T),

b) nonisothermal Von Mises yield function and its associated flow rule,

c) Isotropic hardening or elastic-perfectly plastic behavior.

Both of these models assume no dependence of material properties on cooling rates.

III-B. Properties of HTS

A number of different sources were examined in an attempt to obtain a description of the material properties. These sources included ASTM publications, military specifications, major steel companies, universities, government laboratories and private corporations. In most cases the chemical composition and heat treatment methods had to be compromised to find a similar material with available data. In all cases the data was incomplete for the temperature range of interest. However, the survey was useful in that several organizations that could perform the proper testing were identified.

The HTS plate used in the experiment falls under ASTM designation 537 class 1. Class 1 specifies a normalized heat treatment as opposed to quenched and tempered. Normalizing requires a ferrous alloy to be heated to a suitable temperature above the transformation range and then cooled in air to a temperature substantially below the transformation range. The transformation range is defined by those temperatures within which an austenite structure forms during heating and transforms during cooling. The rate of cooling controls the final grain structure obtained. The transformation range for HTS was taken as 510°C to 760°C and the major property changes that occur are reflected in the variations that occur in this range.

The following discussion will be broken down by individual thermomechanical property. These properties at best represent a compromise from a number of sources.

a) Elastic Modulus (E)

Data supplied by the United States Steel Corporation Research Laboratory for steels with austenitic grain structure show a variation of E at room temperature of from 1.9306×10^{12} dynes/cm^2 (28×10^6 psi) to 2.0685×10^{12} dynes/cm^2 (30×10^6 psi). Some general data on the E variation with temperature was supplied by USS but it did not cover the full temperature range. The data presented in References 6, 7 for HY80 steel was felt to be more accurate and therefore was employed in this study. Figure III-1 contains the assumed variation of elastic modulus with respect to temperature for HTS.

b) Thermal Coefficient of Expansion (α_T)

Data supplied in Reference 8 for α_T for carbon steel was used. This data was available for temperatures less than 650°C (1200°F) and extrapolated far beyond this temperature. The thermal coefficient was assumed to increase linearly from the last known data points

until 760°C. At this point it was assumed to drop to a value that represented 50% of the total change experienced in going from room temperature to 760°C. Although this drop is characteristic of steels, the amount of decrease was completely arbitrary since no data was available. This was simply an attempt to realistically reflect a known fact about the α_T behavior. From 760°C to 1650°C the coefficient of thermal expansion was held constant. Figure III-1 shows the variation of α_T with temperature as used in this study.

c) Yield Stress (σ_Y)

Available data for yield stress for HTS ranged from 3.4475×10^9 dynes/cm^2 (5.5×10^4 psi) to 4.3877×10^9 dynes/cm^2 (7.0×10^4 psi) at room temperature. The low value of 3.4475×10^9 dynes/cm^2 was used for this study. Data was available up to the start of the transformation range at 510°C. The curve from this point on was estimated based upon similar data for HY steels contained in References 6 and 7.

Since no data for hardening modulus (E_T) was available from any of the sources, the material was assumed to be elastic-perfectly plastic. However, data from steels with similar chemical composition and heat treatment showed significant hardening beyond yield, at least at room temperature.

III-C. Idealization of Material Properties

The material properties used in the NONSAP analysis are tabulated in Table III-1. NONSAP is limited to six (6) data points to define material properties as a function of temperature. The program assumes a linear relationship between the data points.

Table III-2 contains the material properties and associated changes in temperature used in the Shrinkage Force Method analysis. The material properties used represent the average for the specified ranges in Figure III-1. Based on the shape of the curves in Figure III-1, three average values for α and E were considered a reasonable approximation. Cool down analysis is assumed to start where the weld metal starts to achieve significant strength chosen somewhat arbitrarily to be about 1400°C.

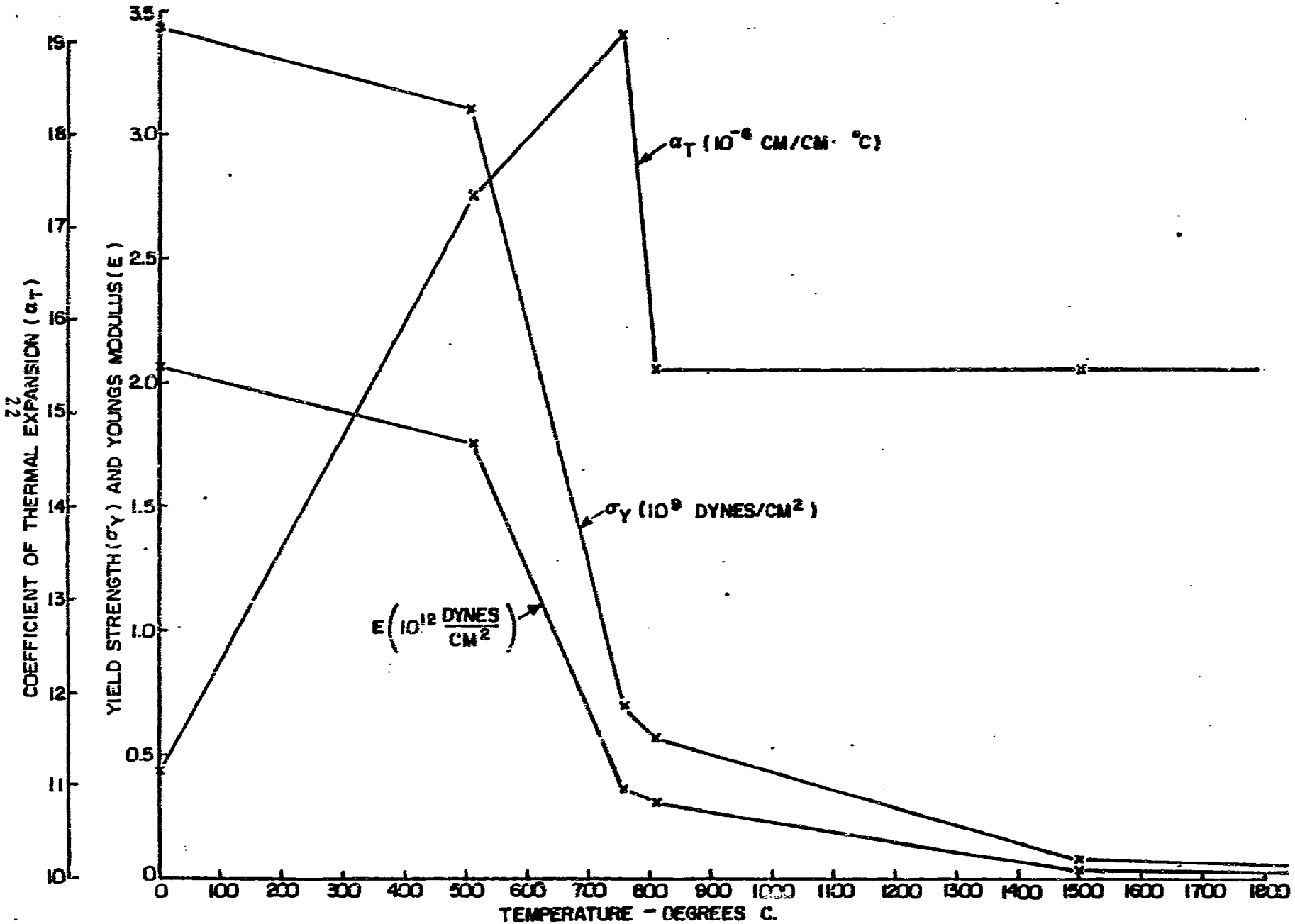

FIGURE III-1 MATERIAL PROPERTIES – HTS STEEL

POINT	TEMPERATURE °F/°C	ELASTIC MODULUS E_F/E_C-psi/μ bar	THERMAL COEFF. α_F/α_C	YIELD STRESS σ_{YF}/σ_{YC} psi/μ bar
1	32/0	$30(10^6)/2.0685(10^{12})$	$6.2(10^{-6})/.1116(10^{-4})$	$5.5(10^4)/3.4475(10^9)$
2	950/510	$25.1(10^6)/1.7306(10^{12})$	$9.63(10^{-6})/.1733(10^{-4})$	$4.52(10^4)/3.11645(10^9)$
3	1400/760	$5.(10^6)/.34475(10^{12})$	$10.6(10^{-6})/.1908(10^{-4})$	$1.0(10^4)/.6895(10^9)$
4	1500/815	$4.4(10^6)/.30338(10^{12})$	$8.58(10^{-6})/.1544(10^{-4})$	$.88(10^4)/.60676(10^9)$
5	2732/1500	$.44(105)/.30338(10^{11})$	$8.58(10^{-6})/.1544(10^{-4})$	$.88(10^3)/.60676(10^8)$
6	5432/3000	0./0.	$8.58(10^{-6})/.1544(10^{-4})$	0./0.

TABLE III-1

MATERIAL PROPERTIES

NONSAP ANALYSIS

TEMPERATURE RANGE (°C)	AVERAGE ELASTIC MODULUS (μ bar)	AVERAGE THERMAL COEFF. (cm/cm-°C)
1371°→760° (Phase 1)	1.7238×10^{11}	$.1544 \times 10^{-4}$
760°C→510°C (Phase 2)	1.0343×10^{12}	$.1822 \times 10^{-4}$
510°C-37.78°C (Phase 3)	1.8961×10^{12}	$.1426 \times 10^{-4}$

TABLE III-2

MATERIAL PROPERTIES

SHRINKAGE FORCE ANALYSIS

IV. APPLICATION OF THE SHRINKAGE FORCE METHOD (SFM) TO WELDING UNRESTRAINED PLATES

IV-A. Introduction

This simplified weld distortion prediction technique is based upon the assumption that the shrinkage forces developed in the weld bead during thermal cooldown are the major contributors to distortion. In the application of the method, the geometry of each weld bead along with the appropriate temperature changes (ΔT) for the cooldown of the bead must be known. In its simplest form the linear coefficient of expansion (α_T) and elastic modulus (E) are used to calculate the linear contraction force bead by bead, and this is applied to the workpiece in a series of numerical solutions for distortions. The following refinements in the procedure over that applied in Reference 2 were incorporated;

a) variable (with temperature) material properties (E and α in the elastic case),

b) detailed workpiece and weld bead geometry representation,

c) actual simulation of weld bead sequence,

d) remelt.

The advantages of the method include;

a) no relatively expensive time dependent nonlinear heat transfer analysis is required,

b) not restricted to the simplified conditions of plain strain or axisymmetric behavior in the workpiece,

c) easy and economical application in "real world" shipyard welding situations.

Although a heat transfer analysis is not required, it may be desirable to obtain a definition of the final solidus-liquidus boundary as a result of each weld pass. This could be obtained from a heat transfer analysis, empirical methods or from experience. Information as to the heat affected zone is also valuable, but not required. This information would assist the analyst in determining the volume of melted material available for shrinkage and the extent to which the high temperatures have altered the structure and thus the material properties of the base metal.

IV-B. Analytical Approach

The various steps in the analysis are defined in the flow chart in Figure IV-1. The flow chart is general in that it includes the steps necessary if the effects of remelt are considered in the analysis. If remelt is not considered, only newly deposited weld metal is assumed to experience thermal shrinkage during the current pass. This material is assumed to have three different elastic moduli (E_i, $i = 1,2,3$) and thermal coefficients (α_{Ti}, $i = 1,2,3$) during the cooldown that occurs in the three steps (ΔT_i, $i = 1,2,3$). Values for E_i, α_{Ti} and ΔT_i are given in Section III-C. The distortion for each weld bead or layer as it cools down is computed. When there is no account for remelt, these displacements are simply accumulated and added bead by bead or layer by layer. The model reflects the changing stiffness and geometry as beads or layers are added. Internal stresses are also accumulated and added throughout the process. When remelt is considered, the internal stresses within the previously cooled material, which is then assumed to remelt, are set equal to zero (i.e. no strength is assumed), and the change in deflection is computed for this condition. The deflection and internal stresses are accumulated for solidification and remelt cycles until the final deformed state is determined.

The approach used in this study idealized the plate as a two dimensional plane strain problem, with zero strain assumed in the direction of welding. As discussed in Section II-C, this assumption appears reasonable in light of the test plate geometry and experimental deflection results. All models employed two dimensional eight noded isoparametric plane strain finite elements. However, the method is not restricted to this geometry and could be applied to axisymmetric geometries or three dimensional solid geometries using the appropriate finite elements.

IV-C. Mathematical Models

Four mathematical models were developed and used to predict the distortion caused by welding the first side of the unrestrained plate. Model 1 consisted of a six layer representation of the weld metal. Figure IV-2 shows the overall model of the plate and the detail of the finite element model in the vicinity of the weld along with the six layers of weld material. One half the plate and weld was modeled with symmetrical boundary condition applied along the line B-F. While the model does include weld joint geometry, it does not consider details of weld bead geometry or remelt effects. From previous studies, six layers is about the minimum number required to produce "converged" final displacements; i.e., using more but thinner layers would yield essentially the same results. While this model is quite simplistic, it is significant because it reflects the types of assumptions that for most practical design or fabrication situations one might be forced to make; i.e., the details of weld bead geometry or extent of remelt are not normally available. For the test plate, a macroscopic cross-section of the weld was photographed at 5 1/2 power magnification. This is shown in Figure IV-3. With this data, it was possible to roughly estimate the weld bead geometry and volume and to include this in formulating model 2 which is shown in Figure IV-4. Due to remelt effects, the macroscopic section does not provide a direct geometric measure of the deposited weld metal. Hence a good deal of judgement and estimating were required.

Model 2 does not assume symmetric response about the centerline (℄). Thus, it was possible to study the effect of non-symmetric application of weld beads on the response. Model 3, shown in Figure IV-5A, considers remelt in addition to weld bead geometry and sequencing. The extent of remelt was estimated from the macroscopic section. Beads 1 and 2 are identified in Figure IV-5B with the cross-hatched area identifying the remelt that occurs in Bead 1 as a result of the deposit of Bead 2. Figure IV-6 shows the entire sequence of weld deposit and remelt cycles used in the analysis to simulate the welding of this joint.

Model 4 represents a change in the weld groove region from Model 3. A refined weld bead geometry was used for Model 4; this is shown in Figure IV-7. The new bead geometry is based upon rough measurements of the fill height after each bead was deposited. Since a continuous profile of upper bead surface was not taken during the test, the bead geometries assumed represent an estimate of what could have existed. However, this is considered an improvement over the weld bead geometries used in Models 2 and 3. A second change between Model 4 and Model 3 is that the cooldown of Bead 1 is ignored, and the analysis starts with the deposit of Bead 2. The experimental results indicated very little distortion for the first bead, and the macrograph (Figure IV-3) provides no information about its geometry. Because of the lack of information and the small amount of distortion associated with Bead 1, neglecting Bead 1 distortion appears to be a reasonable approximation.

For each model, the finite element grid in the weld groove for the entire first side weld is shown in the figures. In fact, during analysis, the model includes only that portion of the weld which exists when any given bead or layer is deposited or remelted.

IV-D. Discussion of Results

1) Model 1

Figure IV-8 contains plots of tip deflection versus weld bead number or corresponding layer number. Also shown are the experimental results. Overall agreement between analytical and experimental results is reasonable with the best agreement occuring for the first beads and the last beads. The changes in deflection or rotation predicted by the intermediate layers underestimates the distortion produced by intermediate beads 4 and 5. The deflection due to completed first side weld is underestimated by about 20%.

Figure IV-9 contains a plot of incremental tip deflections due to each phase of the cooldown cycle for each layer. This plot indicates that all three phases of the cooldown are important, but that Phase 1 has a greater influence for the first layers and Phase 3 the greater influence for later layers.

Table IV-1 compares the results from Reference 2 for one and two constant approximations for the elastic modulus with the results from Model 1 of this study which has a three constant representation of modulus with temperature. The models from Reference 2 utilized a one constant approximation for the coefficient of expansion (α_T) and slightly different temperature

changes were assumed. The table does show, however, the improvement of the distortion results using the simple layer approach with more exact representation of material properties with temperature. The final experimental deflection for welding the first side is also contained in the table.

2) Model 2

Figure IV-10 contains computed incremental and cumulative tip deflections for Model 2. The computed incremental deflections for each bead show best correlation with experimental data for the first four beads and the last two. The deflections due to beads 5, 6, and 7 are underestimated by approximately 50 per cent. The cumulative deflection after completion of the first side is underestimated by approximately 30 per cent, i.e. 1.6 inches versus 1.1 inches.

Computed incremental deflections for each bead and each phase of cooldown is shown in Figure IV-11. Consistent with the Model 1 results, all phases of cooldown are shown to be important contributors to deformation. The last phase of cooldown (Phase 3) has the most significant effect for all beads except number three. For later beads, this result is in agreement with results for Model 1. However, for initial beads or layers Model 1 showed that Phase 1 produced the largest deflections.

This apparent disagreement between Models 1 and 2 results is believed to be due to differences between the two models in geometric representation of, in particular, the first bead. Since the plate is unrestrained, the deformation will be sensitive to the geometry assumed for its first bead or layer, which is quite different for Models 1 and 2. This effect should be considerably less for a restrained structure and in fact the net effect on total cumulative deflections for even this unrestrained plate is not particularly significant. Model 2 results showed no significant non-symmetric response of the plate.

3) Model 3

Figure IV-12 contains computed incremental and cumulative tip deflections for Model 3. The incremental deflections for each bead agree reasonably well with experimental data except for beads 1, 5 and 6. The computed cumulative deflection for completion of the first side welding agrees within a few per cent of the experimental value, i.e. 1.55 inches versus 1.60 inches.

The incremental deflections for each phase of the cooldown are given in Figure IV-13. Consistent with Model 1 and 2 results, all phases are relatively important with Phase 3, the last phase showing somewhat more significance for Model 3.

The incremental deflections due to remelt are shown in Figure IV-14. These results show that remelt causes negative deflections for the first two remelts and positive deflections for the last eight remelts. The magnitude of these effects are small in relation to bead cooldown contributing only about 10% to final deformation.

4) Model 4

The cumulative tip deflections computed with Model 4 is given in Figure IV-15. While the final deflection after bead 9 does not agree with experimental value quite as well as for Model 3, i.e. 1.4 inches versus 1.60 inches, the shape of the curve and incremental deflections for each bead are judged to be in better overall agreement. This overall improvement is believed to be due to a better geometric and volume approximation to each bead. This was made possible by use of both the macroscopic section of the completed weld and rough measurements of the depth of fill after each bead was laid down. As stated in Section IV-C, only the macroscopic section data was used to estimate the weld bead geometry and volume for Models 2 and 3 which is not sufficient for an accurate representation.

5) Summary

The calculated tip deflection for Models 1 through 4 and the measured experimental results are shown on Figure IV-16. Model 4

is considered to be in best overall agreement with experimental and Model 2 the worst. However, all models provide reasonably good estimates of the final deflection for the completed first side weld.

The shape of the deflection curve versus bead number is best approximated by Model 4 which is considered to have the most accurate representation of actual weld bead geometry, and which also includes the effects of remelt.

Model 1, which assumes a layered weld metal deposit and no remelt effects, still provides reasonable accuracy for this problem.

There was no clear-cut improvement in accuracy obtained in going from Model 1 to Model 4, even though each model, in succession, appeared to be better than the previous model. Two possible explanations come to mind: 1) the detailed buildup of the weld bead profile is not known, possibly leading to an erroneous conclusion about the "goodness" of the respective models; and 2) because of the assumptions and simplifications of the "shrinkage force" analytical approach, as applied to this problem, the type of model refinement attempted here may not be meaningful.

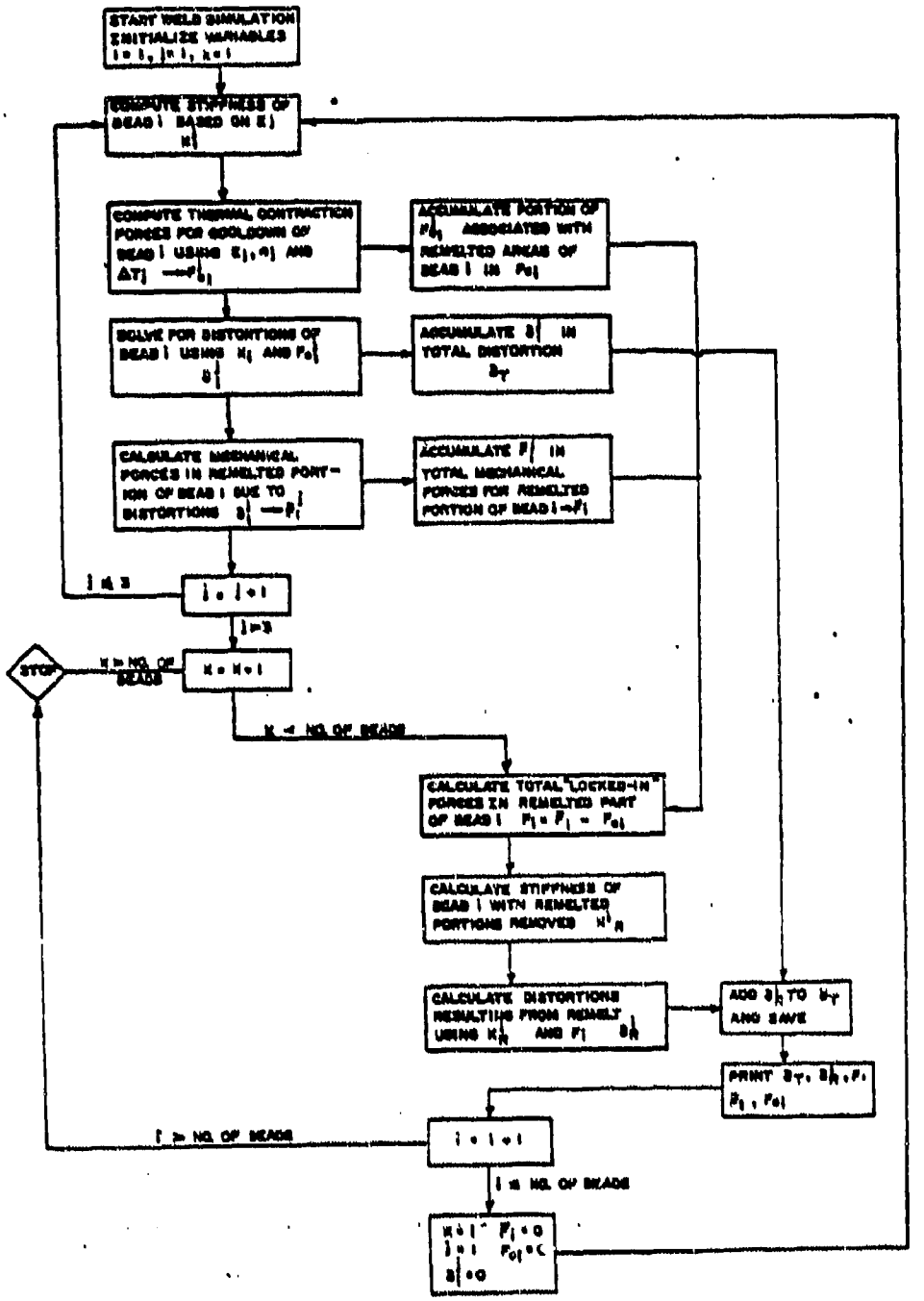

GENSAM SIMULATION FLOWCHART

FIGURE III-1

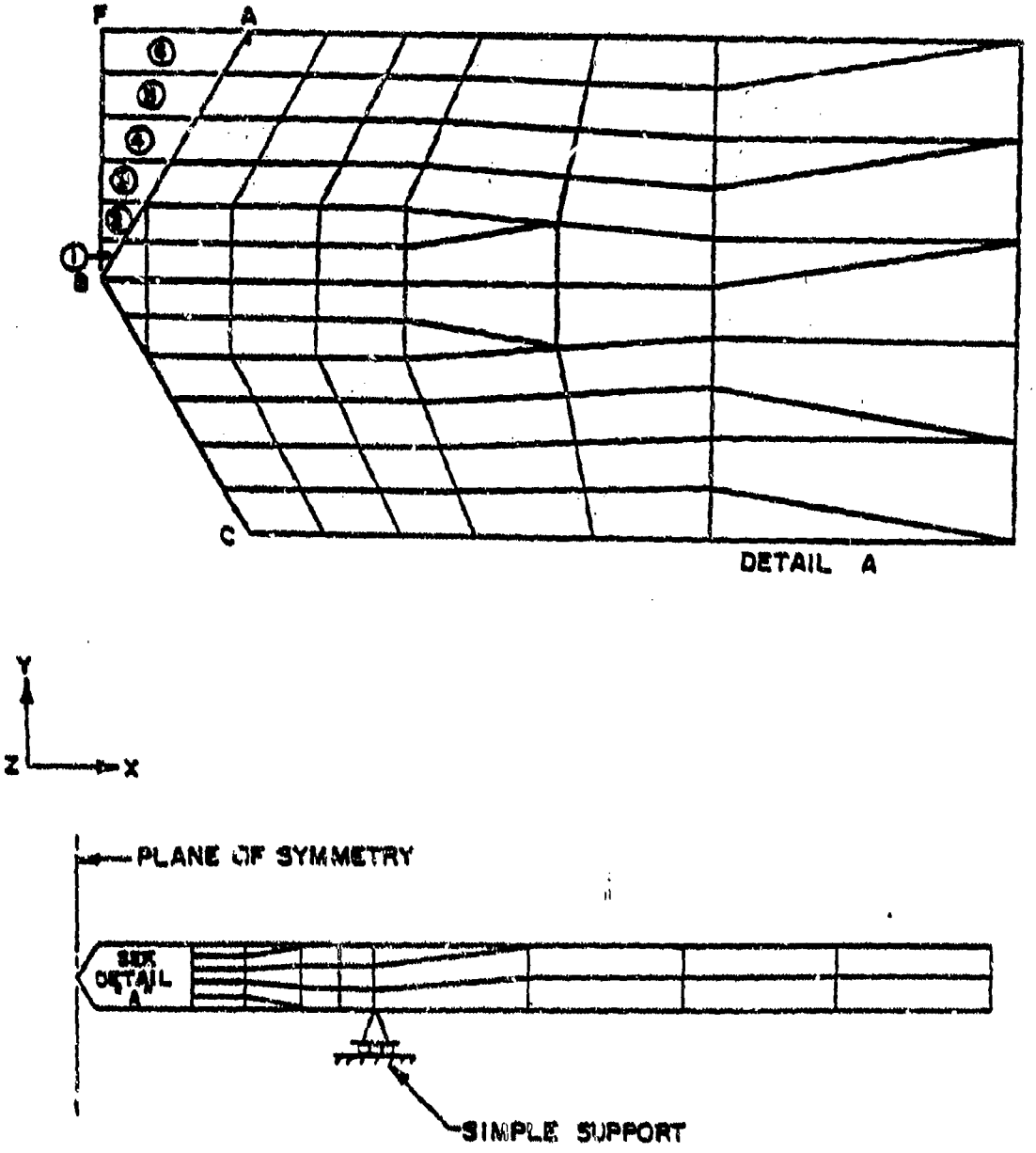

FIGURE IV-2 MODEL 1

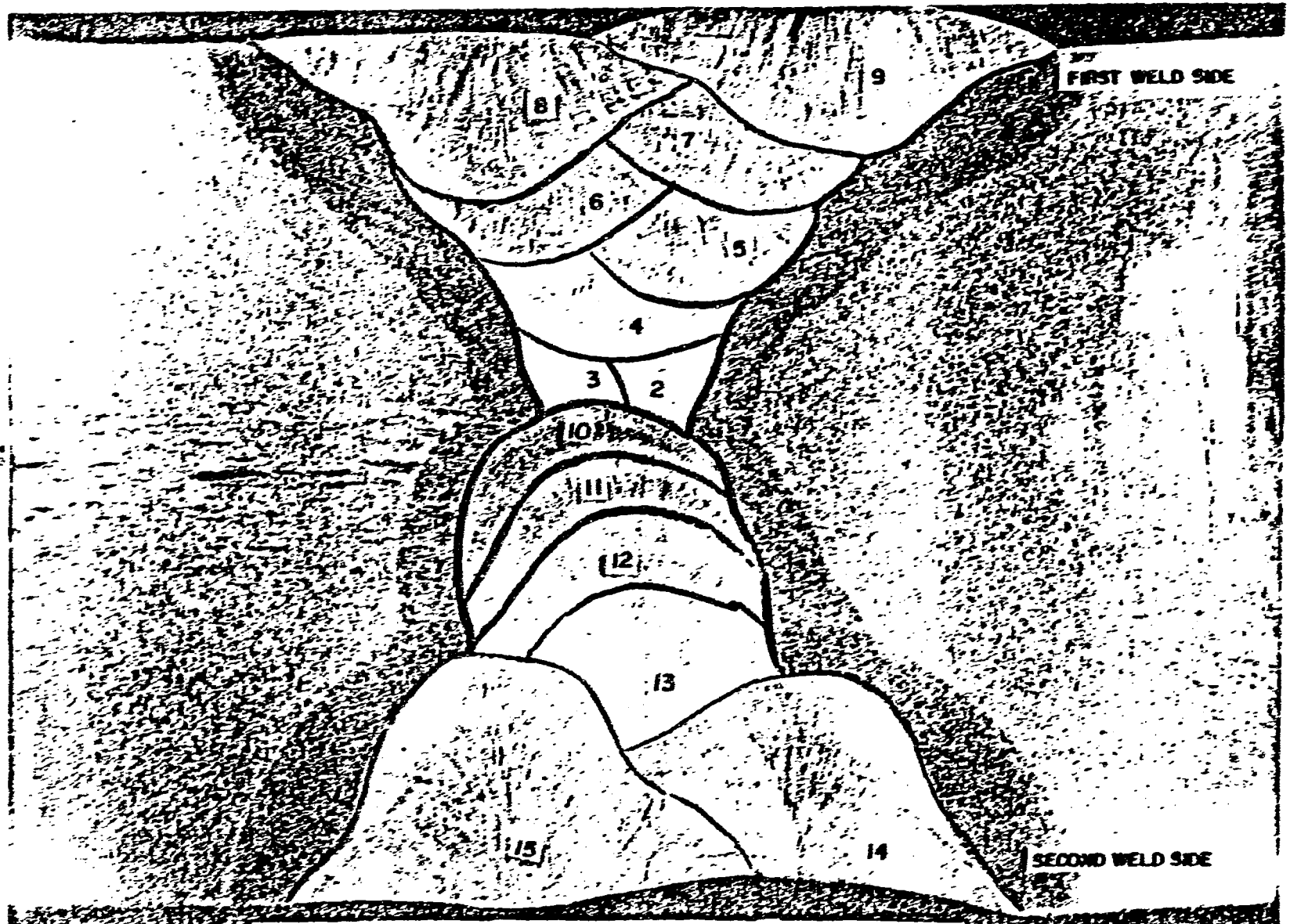

FIGURE IV-3 MACROSCOPIC CROSS-SECTIONAL VIEW at 5 1/2 X

THIS PAGE IS BEST QUALITY PRACTICABLE
FROM COPY FURNISHED TO DDC

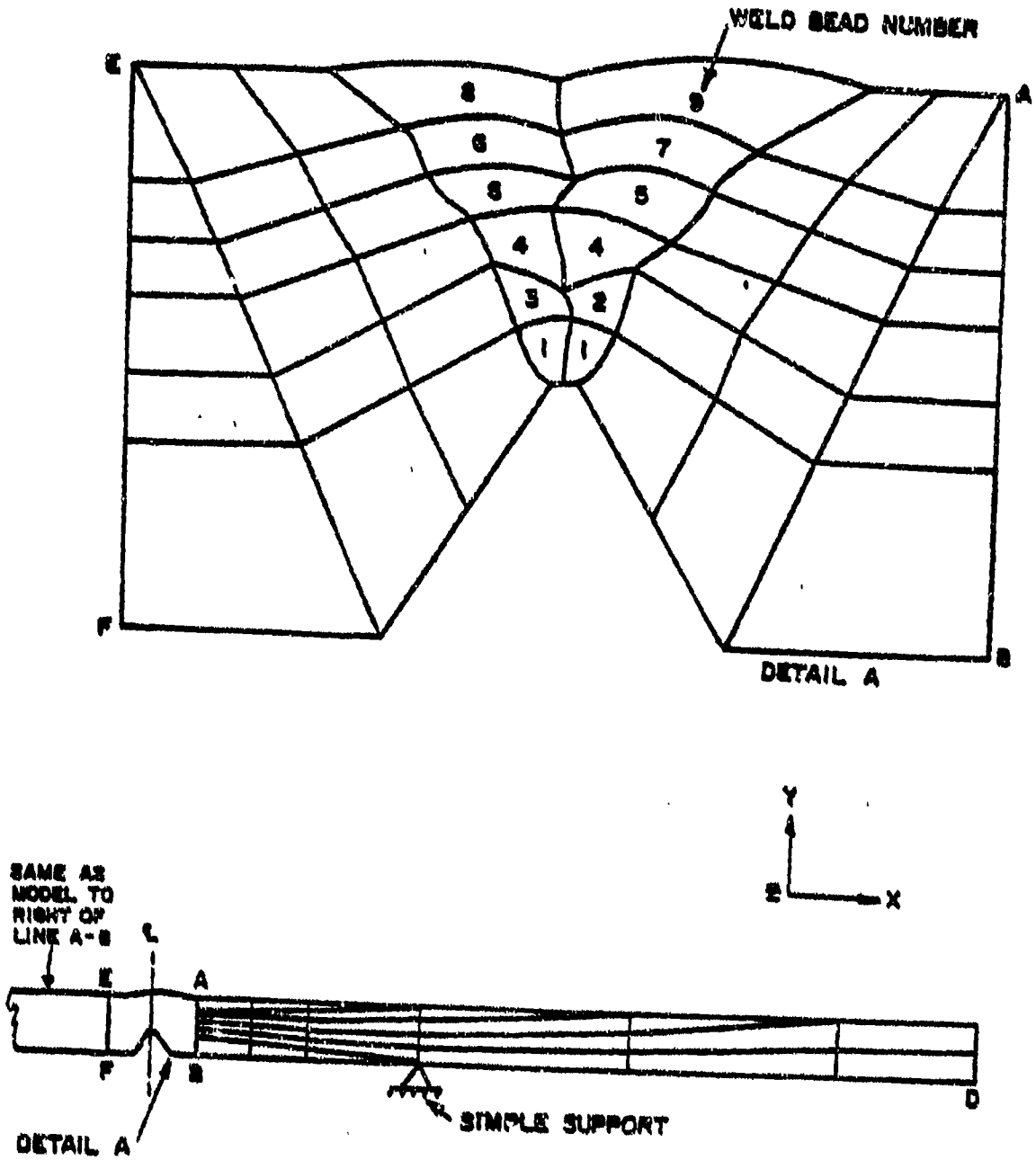

FIGURE IV-4 MODEL 2

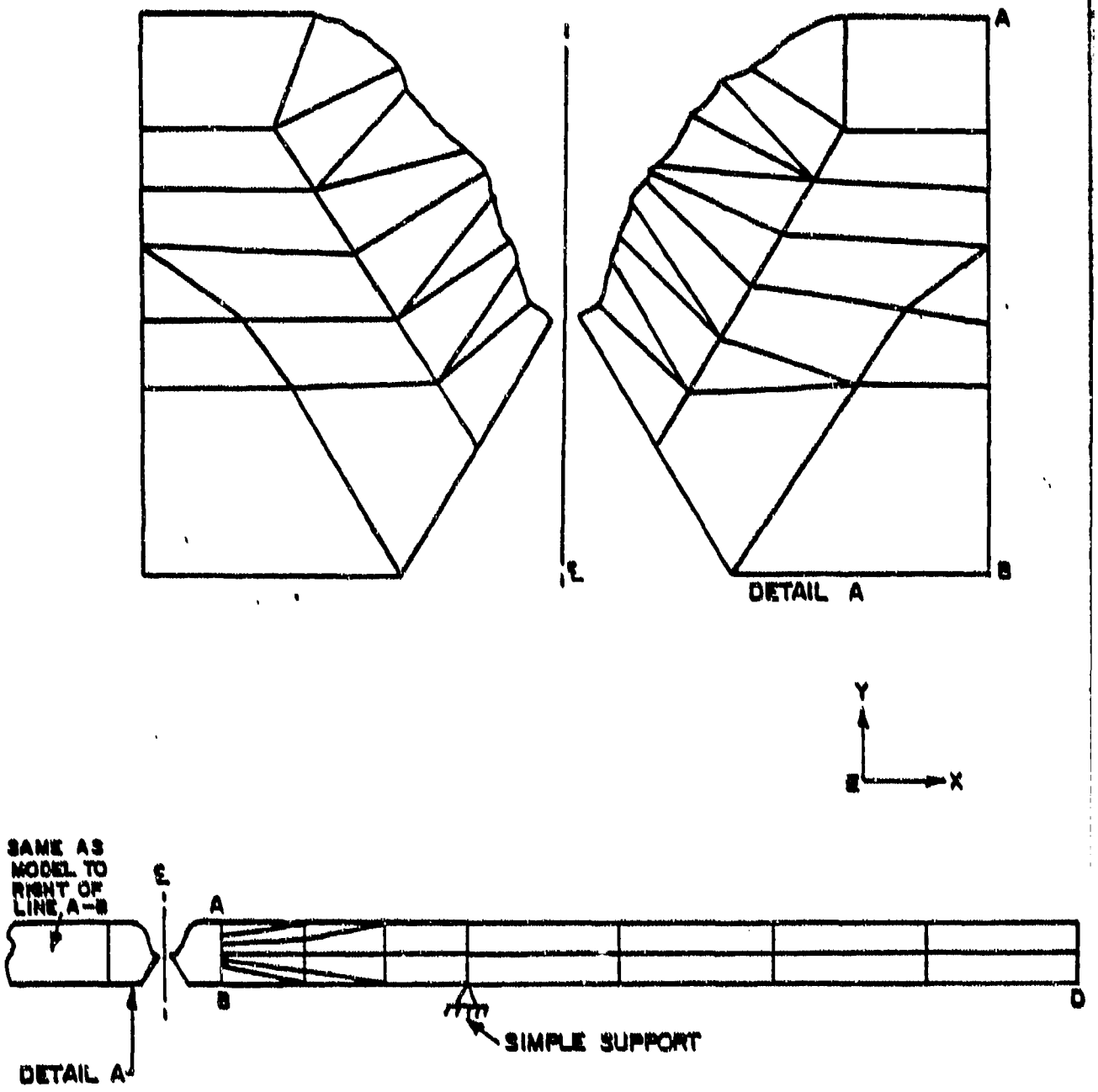

FIGURE IV-5A MODEL 3

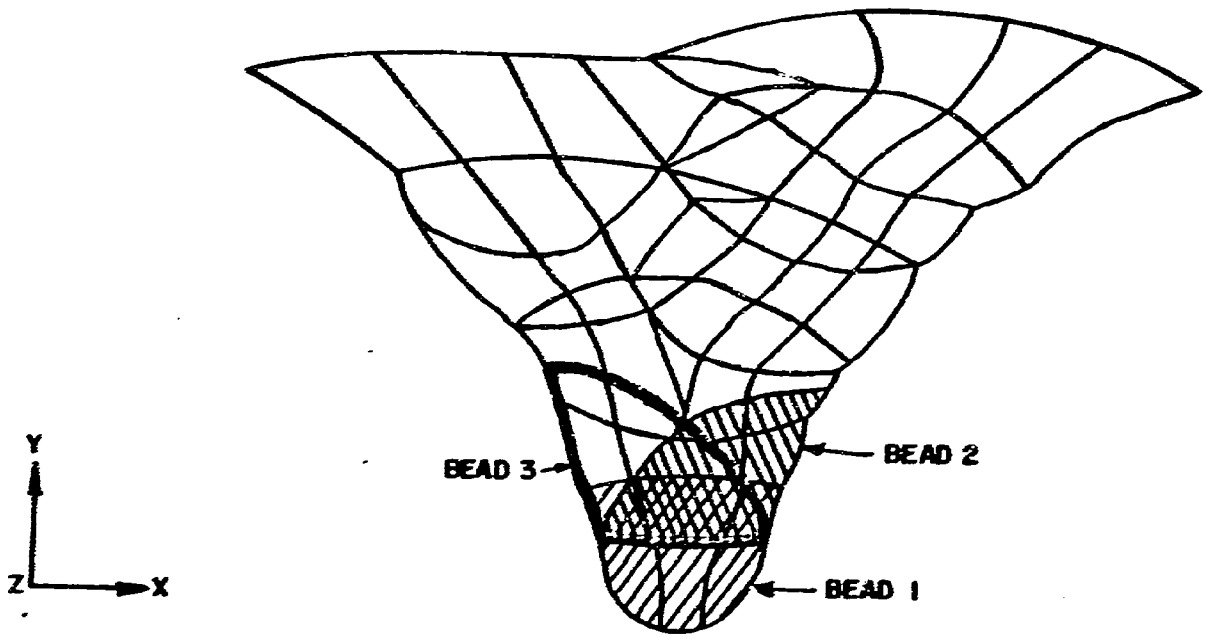

FIGURE IV-5B WELD GROOVE REGION - MODEL 3

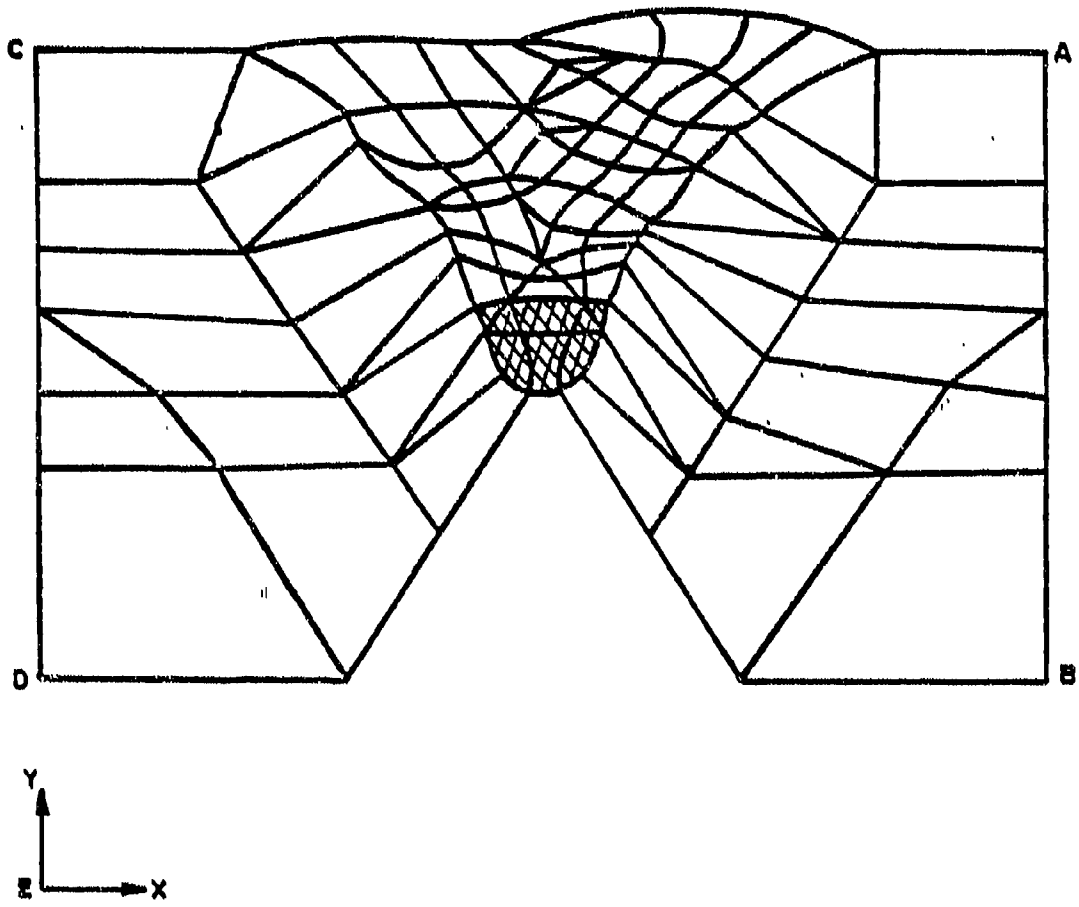

FIGURE IV-6A BEAD 1 DEPOSIT

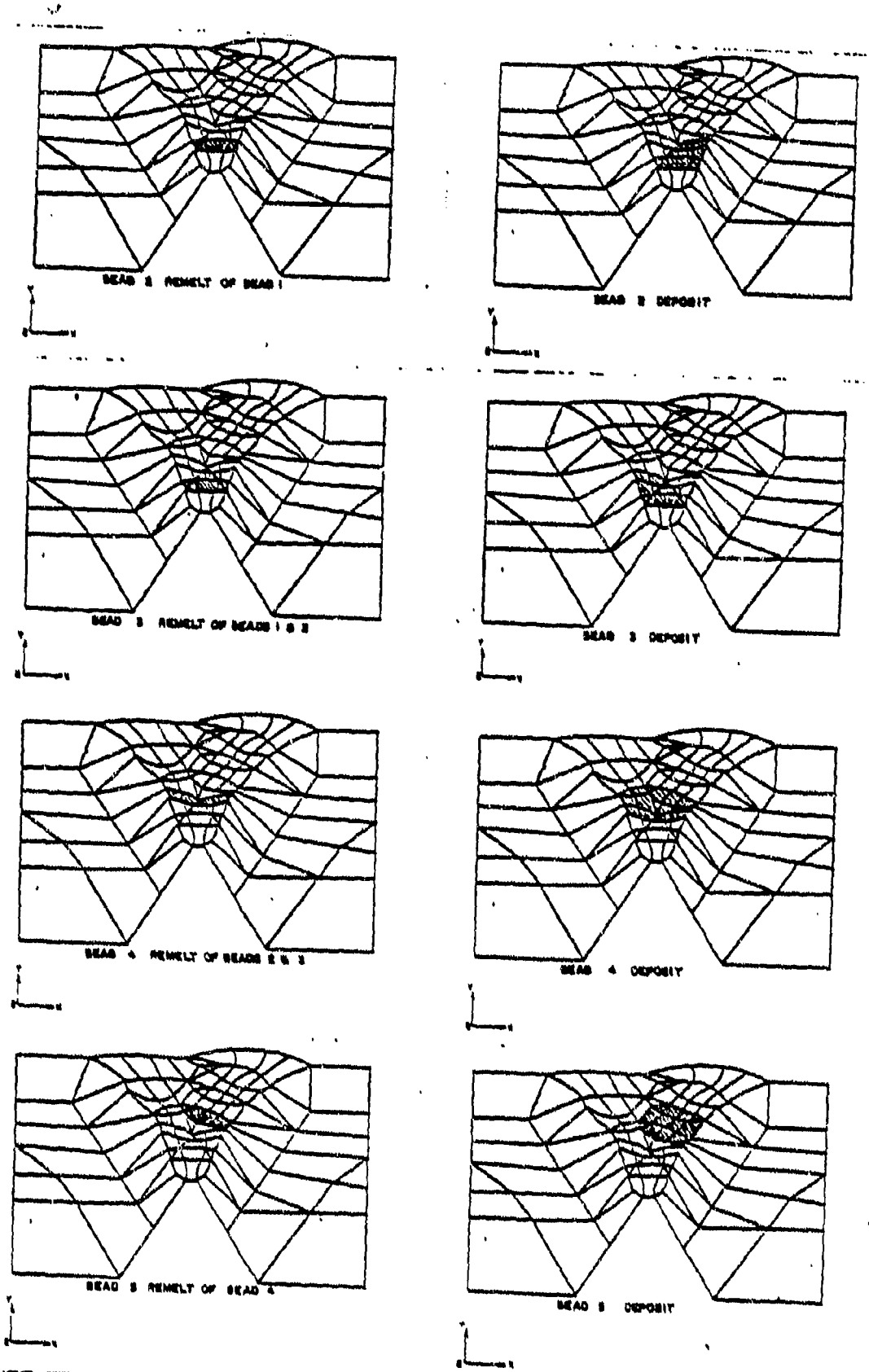

FIGURE IV-6B WELD DEPOSIT AND REMELT BEADS 2 THROUGH 5

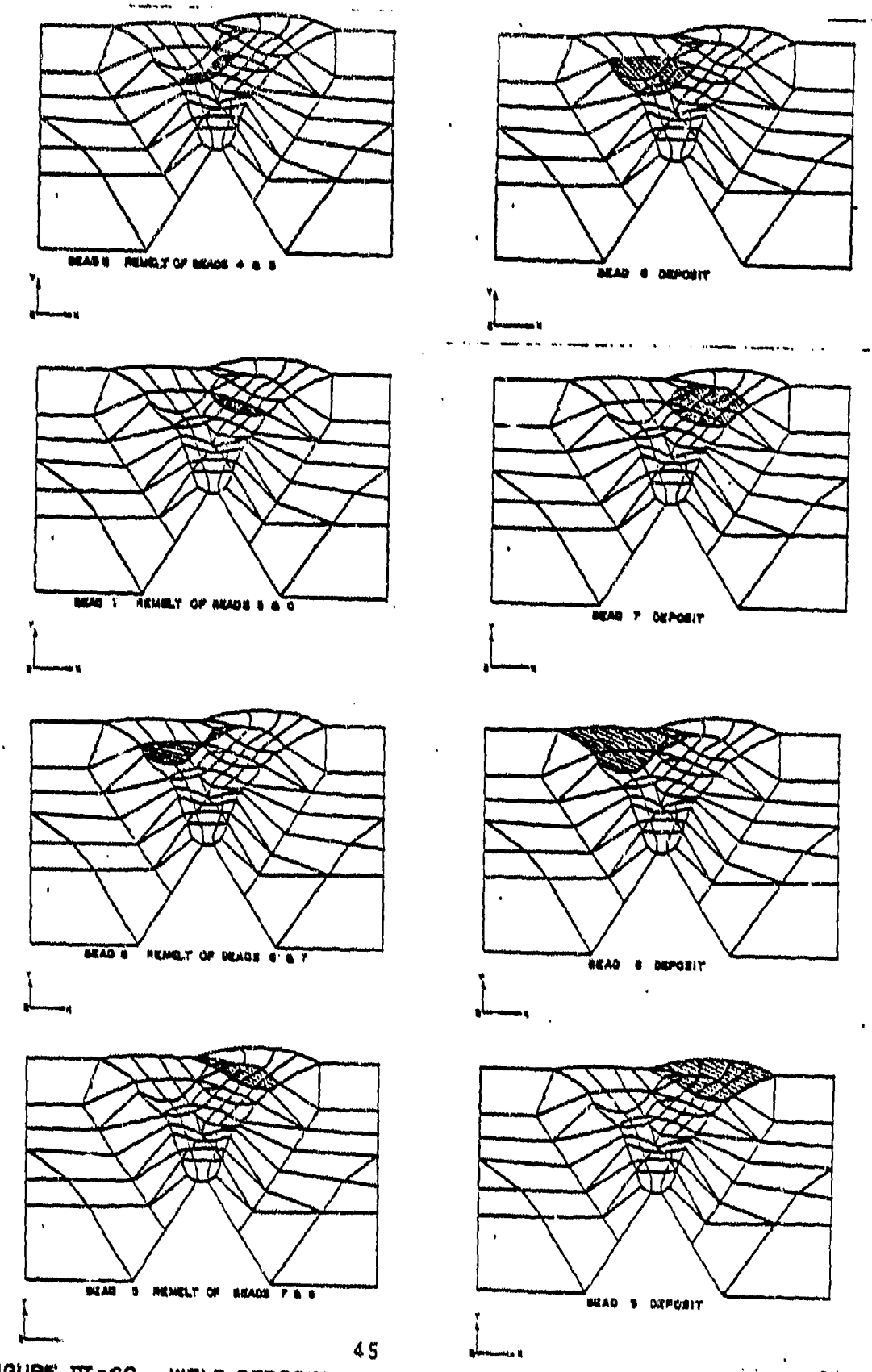

FIGURE IV-6C WELD DEPOSIT AND REMELT BEADS 6 THROUGH 9

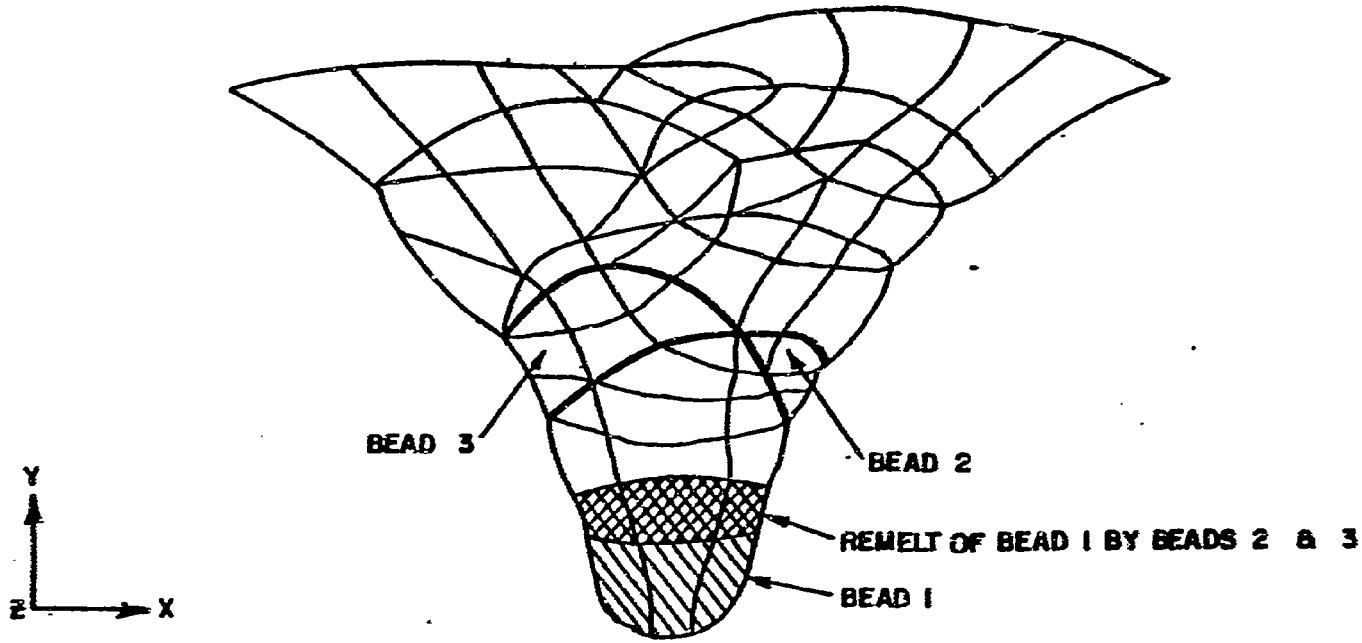

FIGURE IV-7 MODEL 4 - ALTERNATE WELD BEADS WITH REMELT
(REST OF PLATE MODEL IDENTICAL TO 3)

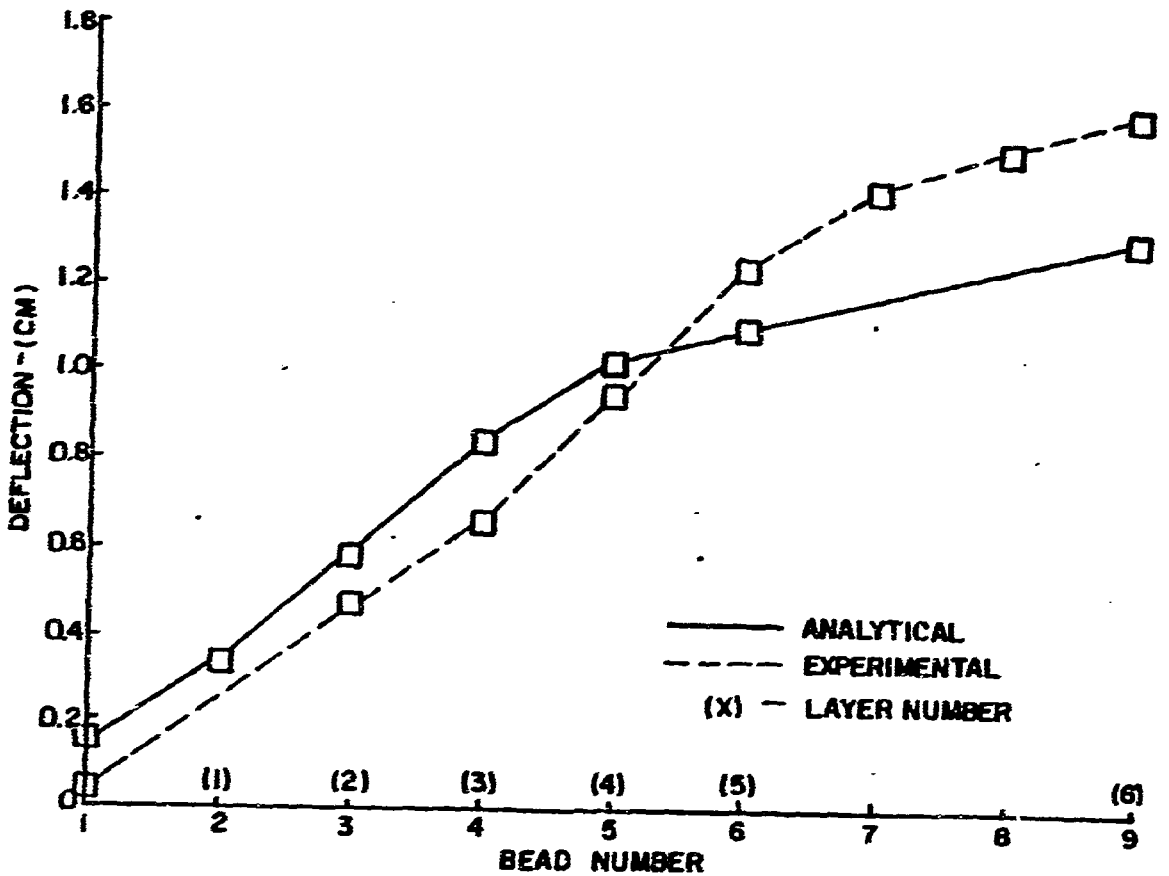

FIGURE IV-8 TIP DEFLECTION vs. BEAD NUMBER
MODEL I

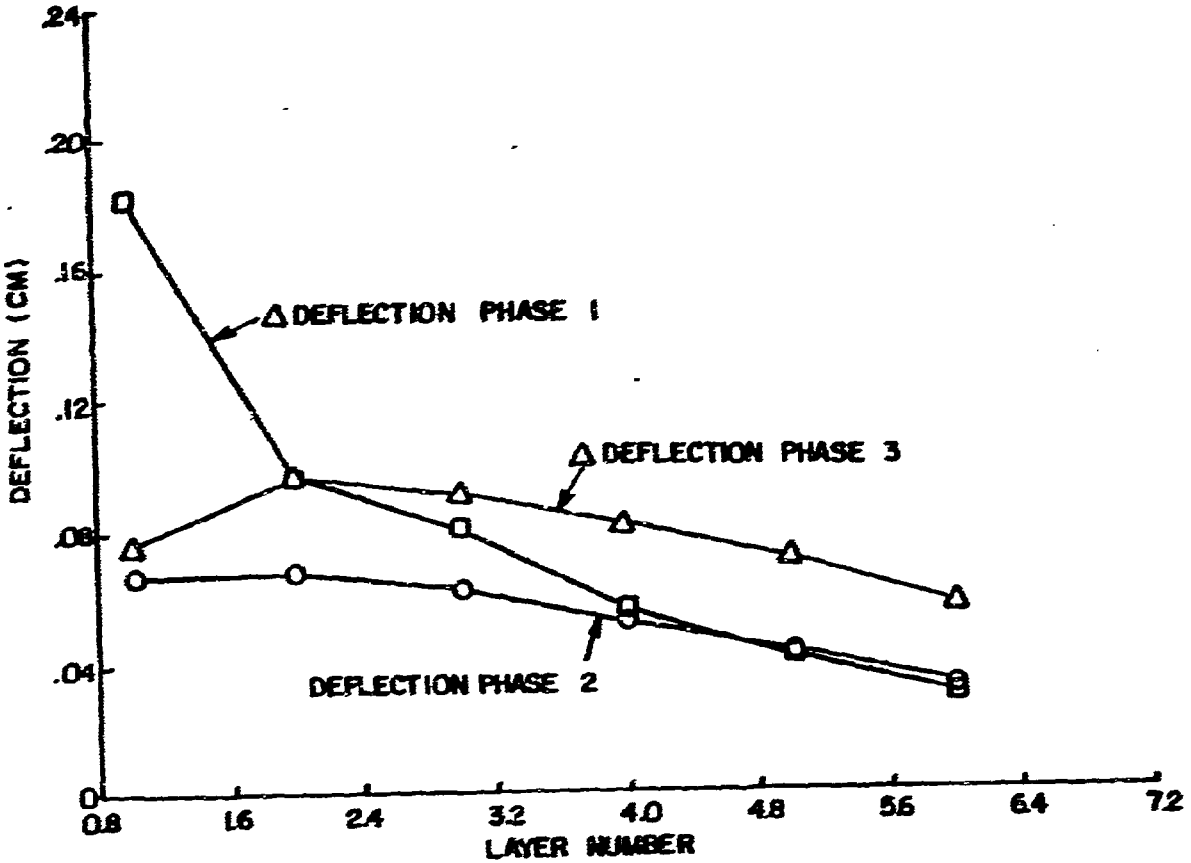

FIGURE IV-9 PHASE DEFLECTIONS vs LAYER NUMBER
MODEL 1

TIP
DEFLECTION (CM) MODEL 1

LAYER	LINEAR* E	BILINEAR* E	TRILINEAR E, α_T	EXPERIMENT
1	.1895	.1757	.3254	
2	.3973	.3853	.5867	
3	.5910	.5849	.8221	
4	.7508	.7582	1.0141	
5	.8814	.9053	1.1704	
6	.9830	1.023	1.2904	1.6094 (Final)

*Reference 2

TABLE IV-1

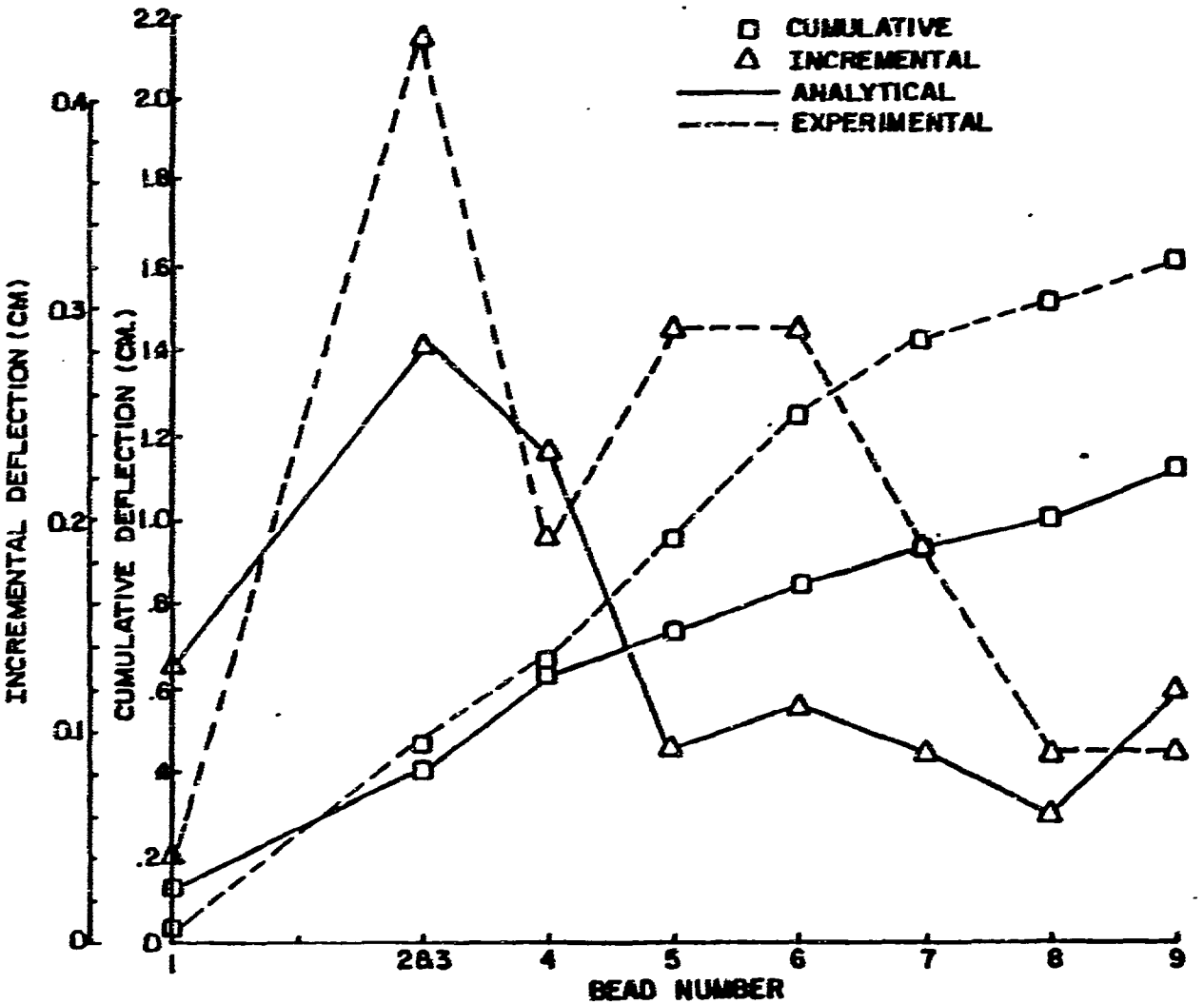

FIGURE IV-10 CUMULATIVE AND INCREMENTAL TIP DEFLECTION vs BEAD NUMBER - MODEL 2

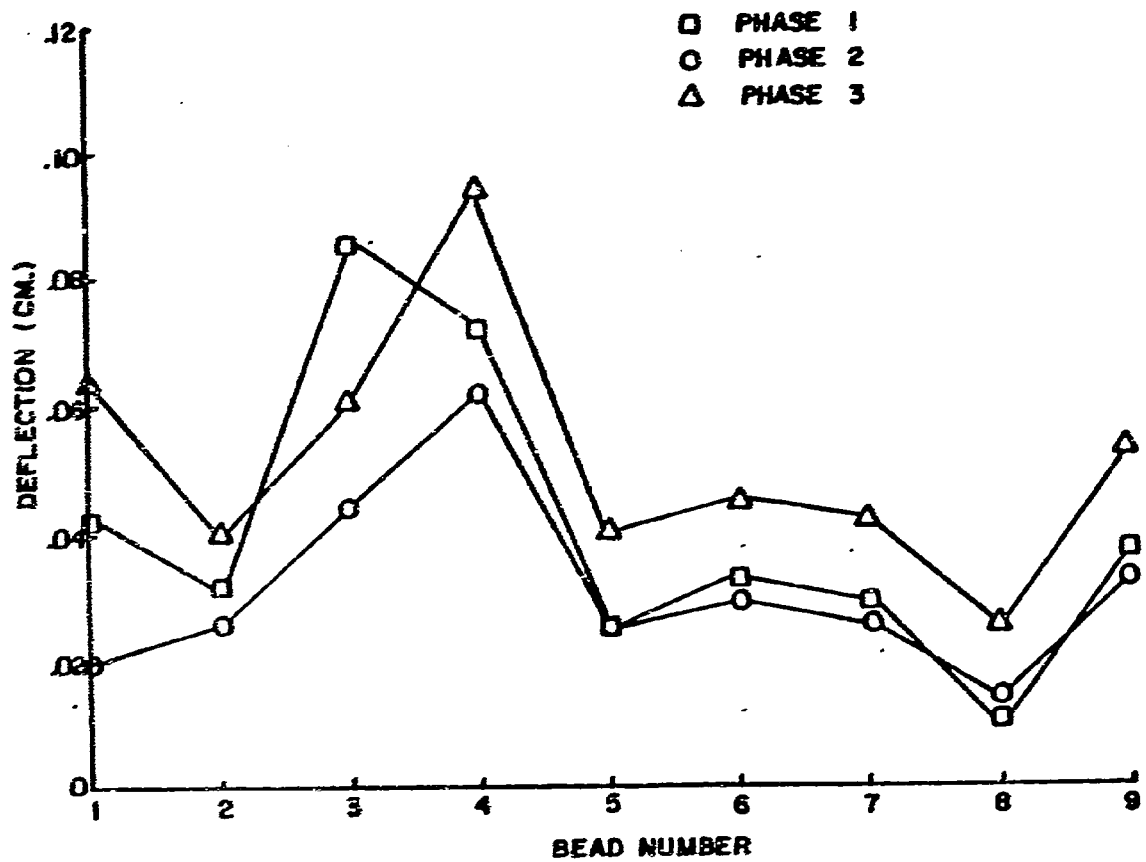

FIGURE IV-11 PHASE DEFLECTIONS vs BEAD NUMBER – MODEL 2

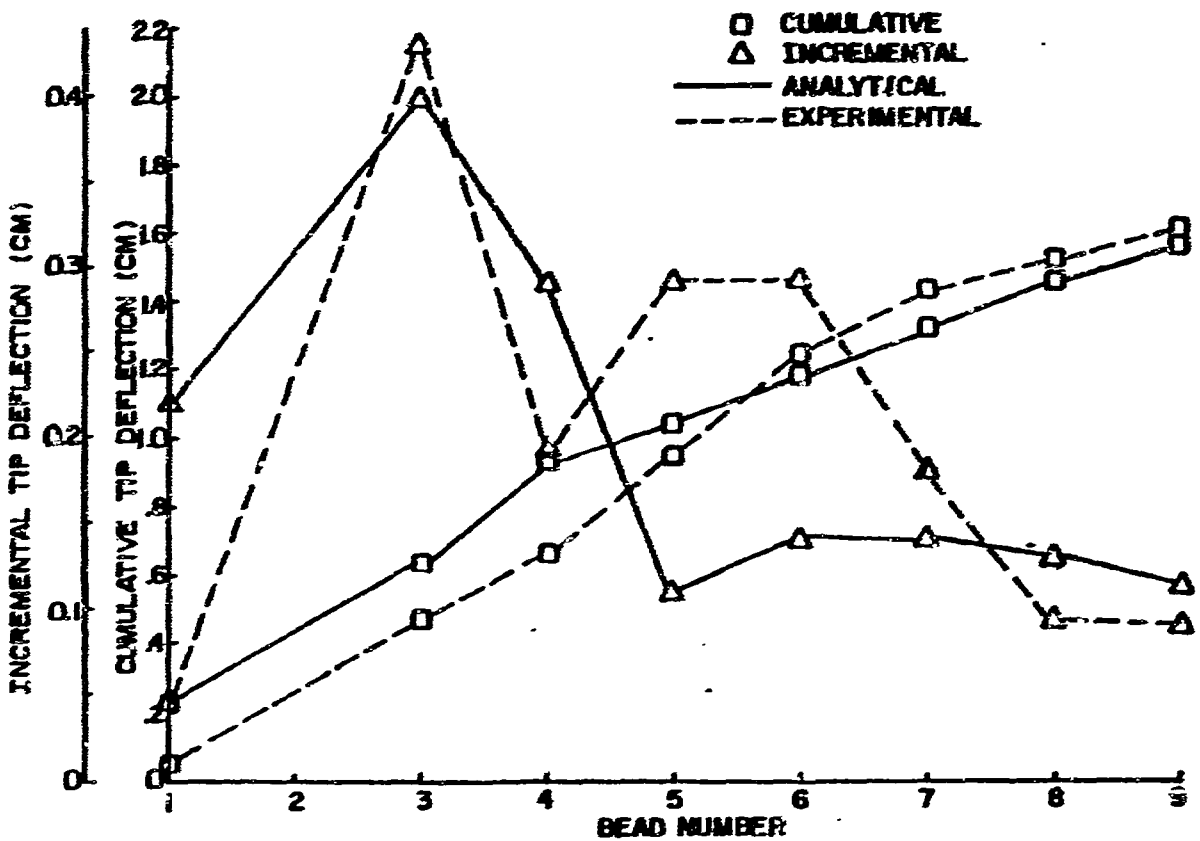

FIGURE IV-12 CUMULATIVE AND INCREMENTAL TIP DEFLECTION vs BEAD NUMBER - MODEL 3

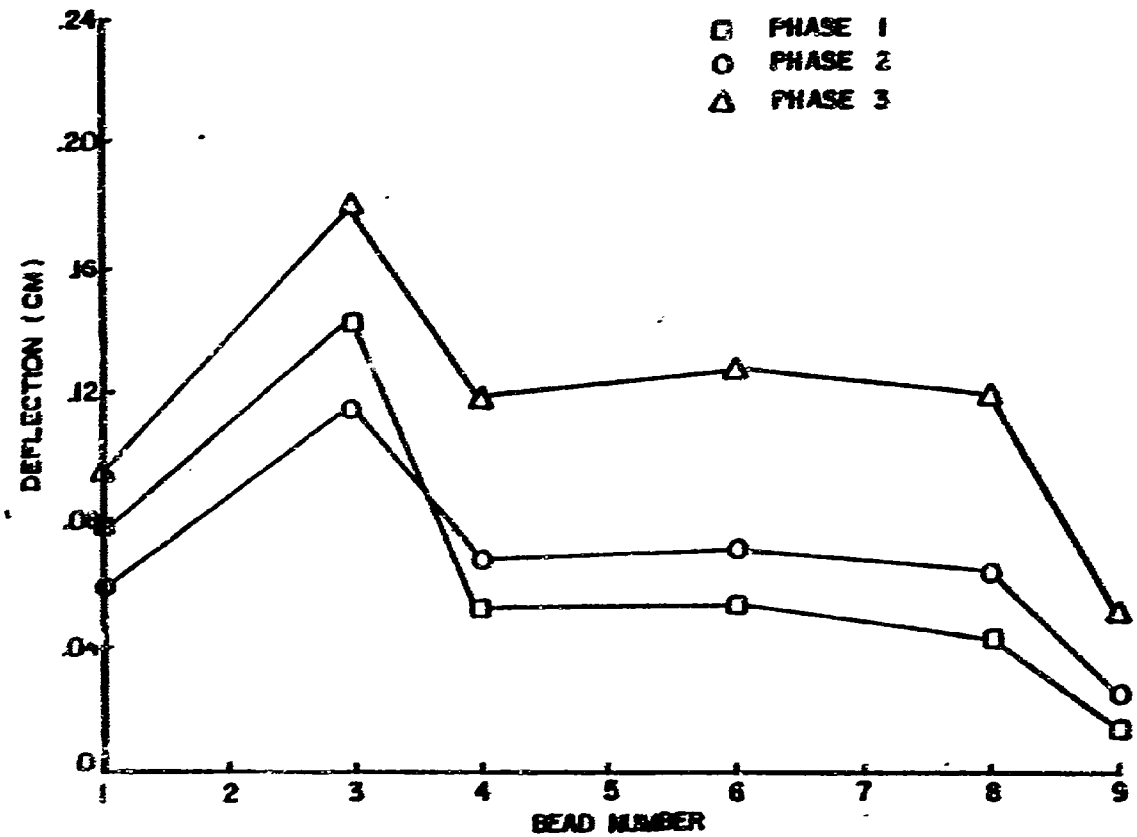

FIGURE IV-13 INCREMENTAL PHASE DEFLECTIONS vs BEAD NUMBER - MODEL 3

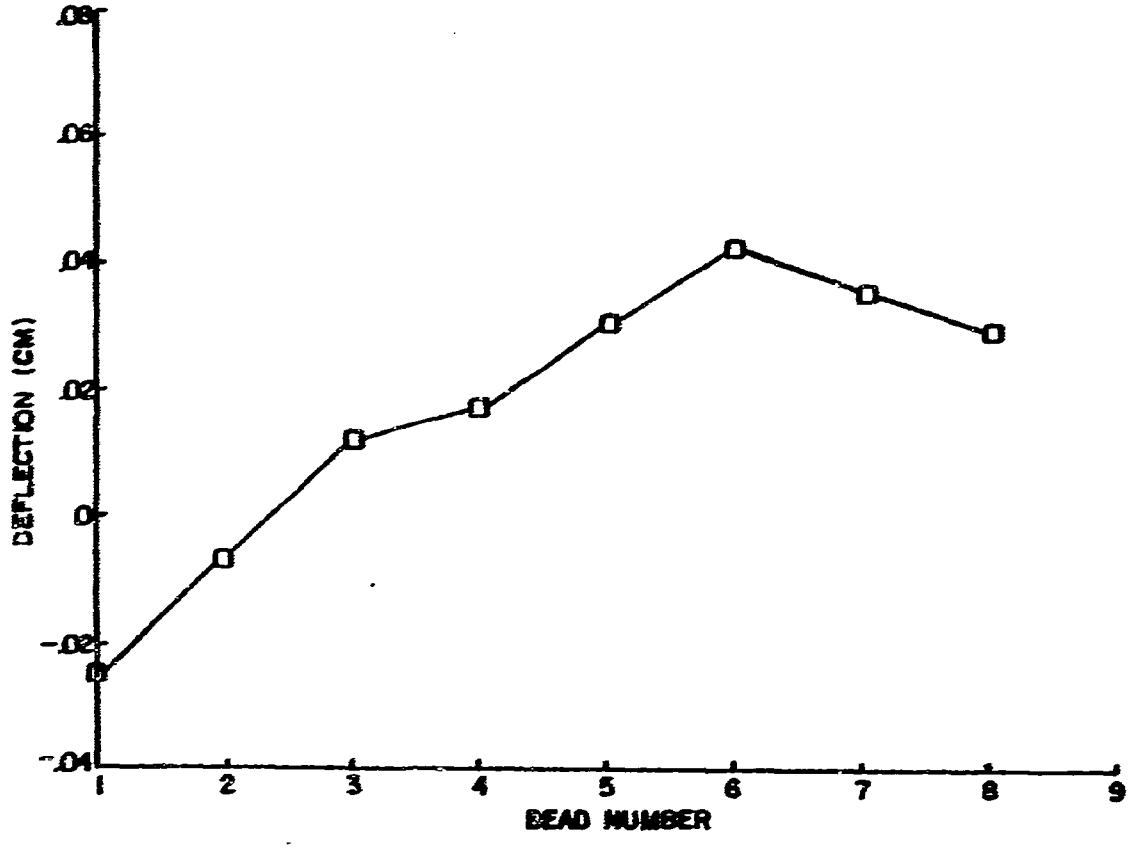

FIGURE IV-14 INCREMENTAL DEFLECTIONS DUE TO REMELT vs BEAD NUMBER - MODEL 3

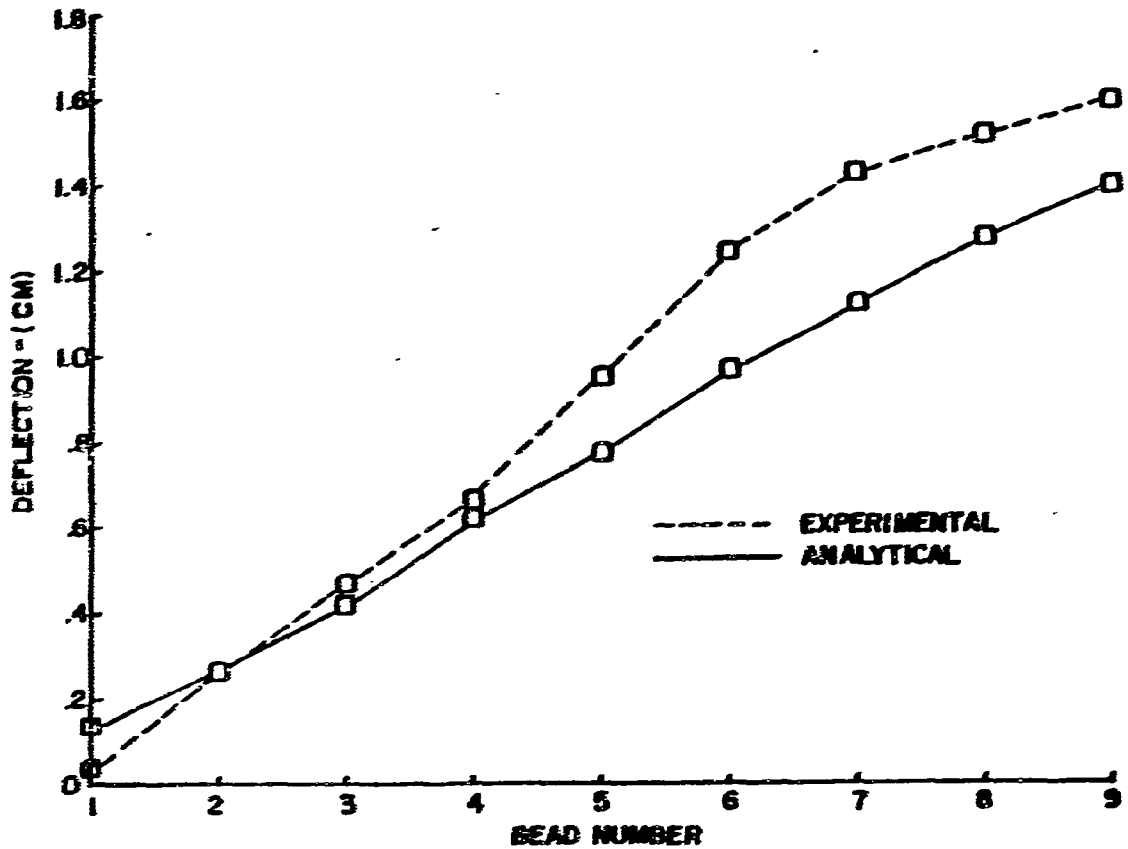

FIGURE IV-15 CUMULATIVE TIP DEFLECTION vs BEAD NUMBER
MODEL 4

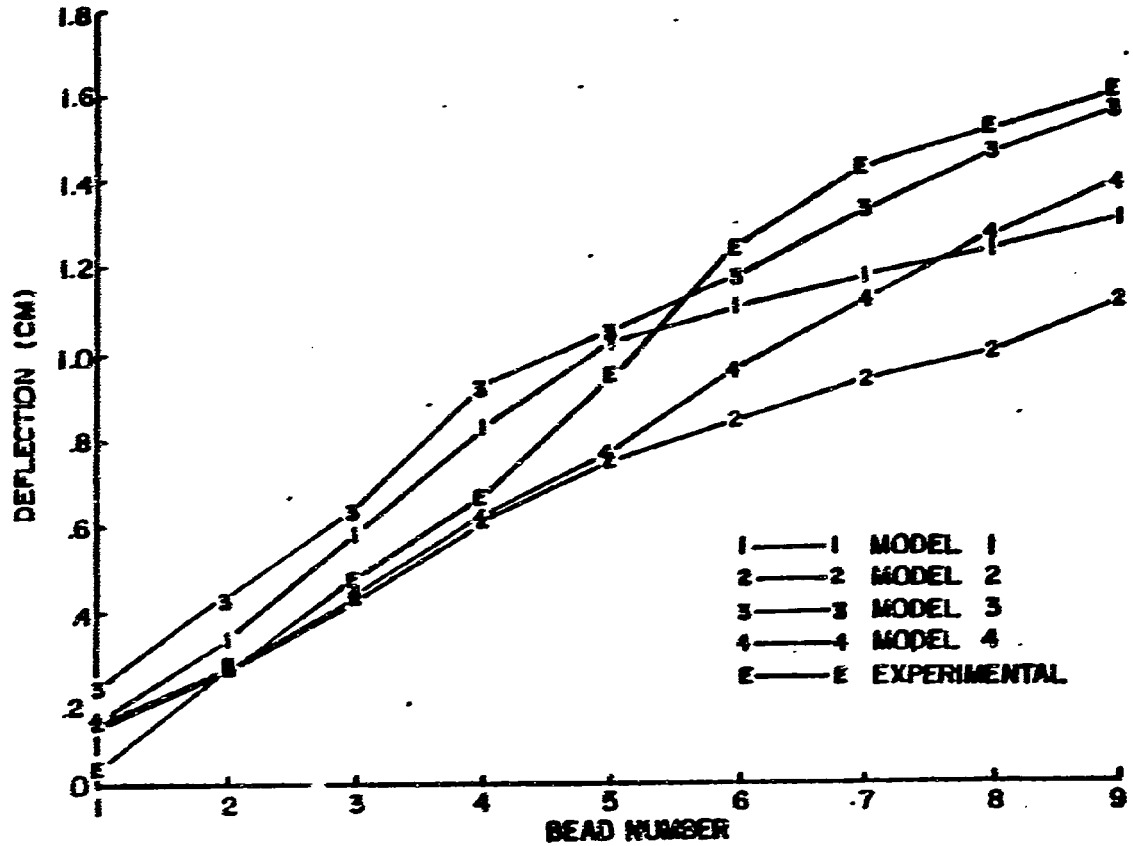

FIGURE IV-16 TIP DEFLECTION vs BEAD NUMBER
MODELS 1,2,3,4

V. APPLICATION OF THERMOPLASTIC ANALYSIS TO WELDING UNRESTRAINED PLATES

V-A. Introduction

Assuming one starts with a validated computer code, which possesses the necessary analytical capabilities to conduct a welding-simulation analysis, the accuracy of the solution will be controlled by three basic inputs:

1) applied loading
2) material stress-strain behavior model
3) mathematical discretization of structure.

If one were performing a static linear elastic stress analysis of a pressure vessel, the first two inputs are straightforward and the only real work involves the third input. However, in welding-simulation analysis all three inputs pose real problems for the analyst. There is insufficient experimental data available to define the first two inputs with certainty. The degree of experimental sophistication required for measurement of welding-induced phenomena is significantly beyond that required to measure Young's Modulus. Also, because of the high computer run cost for transient, welding-simulation

analyses, the number of degrees of freedom in the mathematical discretization can dictate whether an analysis is attempted or abandoned as too costly. The effect of this is to severely limit the conduct of modelling studies as a check that the mathematical discretization of the structural geometry is adequate.

The present state-of-the-art appears to be 1) "best-guess" time-dependent temperature distributions; 2) applied to a structure with "best-guess" temperature-dependent material properties; and 3) discretized mathematically by an economically feasible number of degrees of freedom. This reality makes evaluation of the basic analytical capability, as represented by a computerized analytical procedure, extremely difficult since lack of agreement with actual measured response could be caused by incorrect input, by inadequate theoretical formulation, or by both. Also possible is the situation where the interaction of a number of inaccuracies may coincidentally appear to produce accurate results when compared to measured data.

With these considerations in mind, application of the NONSAP computer code to transient, thermo-plastic analysis of welding-induced behavior should be viewed more as a feasibility and qualitative evaluation, than as a quantitative evaluation for correlation to experimental results.

The NONSAP finite element program was modified in 1977 to perform thermoplastic analysis with temperature dependent material properties (Reference 2). Additional modifications were made in 1978 to assist in the analysis of weld distortion problems. Specifically, a "birth" and "death" option has been added for the two dimensional finite elements representing the weld deposit. At predetermined times in the analysis, elements in the weld groove region can be born (achieve strength from cooldown) or die (melt). This feature assists in modelling of the weld bead.

One of the difficulties encountered in the analysis of unrestrained butt welded plates, supported on knife edges, is that the plates are basically free to rotate as rigid bodies during the weld process. Thus, during welding, the plates lift off one of the 2 sets of supports; therefore, a nonlinear support with large compressive stiffness and essentially zero tensile stiffness had to be simulated. This was accomplished using 1-D truss finite elements with elastic, nonlinear material properties. With the required program development completed, the analysis of the experiment described in Section III was initiated.

Transient temperature distributions in the plates for deposit of weld beads 1 and 2 were calculated in 1977 using the TEMP

computer code (see Reference 2). These were used in 1978 as input to NONSAP for the analysis of distortion caused by deposit of assumed weld layers 1 and 2.

The weld layer geometry for the NONSAP analysis is the same as that used in GENSAM Model 1, described in the previous section. A detailed weld bead definition, such as was used in GENSAM Models 2, 3, and 4, was not attempted in the NONSAP analysis. The lack of detailed weld bead description in the NONSAP model increases the difficulty of interpreting and evaluating the results obtained, since there is not a one-to-one correspondence between the analytical model and the experimental model for either weld layer 1 or weld layer 2. This choice of weld bead description was made based on concern for computer run cost and the limitation on degrees of freedom in NONSAP, which uses an in-core solution technique. More detailed (and correspondingly more expensive) models could be analyzed using the ADINA computer code, which is a general purpose code, based on NONSAP, developed by Prof. Bathe at MIT.

V-B Analysis Methods

Figure V-1 shows the overall NONSAP finite element model used for the thermoplastic analysis. The simple supports at A and B have been replaced with a spring trusswork. These supports have the ability to roll freely in the Y direction and constrain translation in the -Z direction. This is accomplished by specifying nonlinear properties for the truss members. This mechanism for the supports generally worked well. Figure V-2 shows the model of the weld groove region used in the NONSAP analysis. Translational motion in the Y direction was constrained at the weld centerline (AB). Both Layers 1 and 2 are shown in Figure V-2; however, their births occur at different times during the analysis and their mutual presence in Figure V-2 is purely illustrative.

Four-noded isoparametric, quadrilateral, plane-strain finite elements, with a 2x2 Gaussian integration scheme, were utilized in the analysis. The elements were reduced to triangular shapes where necessary, to represent the geometry and for transition from large element size to small element size as the weld region is approached.

While the grid is significantly refined in the weld region, it is still too crude to represent the detailed thermo-plastic stress behavior of the weld metal and adjacent plate. To accurately predict these stresses during and after welding, the element density would have to be 5-10 times greater for the elements used. However, as a demonstration problem, to determine the overall distortion behavior of the plate, the element density was judged adequate.

The only load on the plate, other than the transient temperature distribution caused by welding, is the dead weight of the plate itself.

From the transient heat transfer analysis, a file of nodal temperature distributions as a function of time were generated to simulate the heatup-cooldown cycle caused by deposition of weld layers 1 and 2. For the NONSAP analysis, a sequence of temperature distributions was chosen from this output, such that the maximum temperature change at any node in going from time (i) to time (i+1) was $|\Delta T| \leq 200°C$.

From the nodal temperatures, the temperature at the four Gauss points in each finite element is calculated in NONSAP. The

tangent stiffness is then calculated, using the material properties associated with the current temperatures and stresses at the Gauss points. The increment of Thermal Load in going from time (i) to time (i+1) is applied to obtain the increment in nodal deflections and the associated incremental stresses at the Gauss points, assuming elastic behavior. Then the total stress at each Gauss point is compared to the Von Mises yield surface at the current temperature to determine whether the increment in stress calculated elastically is admissible or whether the yield surface has been exceeded. If the yield surface has been exceeded, the stresses are adjusted to be consistent with the specified plastic behavior model.

Equilibrium iterations are performed until the displacement solution has converged to within a .005 error tolerance. Within each iteration, the stresses are updated, checked against the yield surface, and corrected if necessary.

V-C. Analysis Results

Figure V-3(a) shows the average temperatures of Weld Layers 1 and 2 during the analysis and Figure V-3(b) shows the tip deflection of the plate during the analysis. The solution for Layer 1 deposit had 25 load (temperature) steps and the solution for Layer 2 deposit had 44 load steps.

The initial approach was to analyze one temperature sequence, including the two heatup-cooldown cycles and introducing the Weld Layers 1 and 2 at the appropriate times. This approach had to be abandoned when, during the heatup for Layer 2, unresolvable convergence difficulties developed. As the temperature of the previously deposited Layer 1 increased, during the 2nd heat-up, the yield strength of Weld Layer 1 decreased to the point where the plate deflection could no longer be supported, and consequently the deflection rapidly reduced toward zero. A displacement solution showing the plate settled back on the supports was obtained, but the reaction forces at the supports were grossly in error. While considerable effort was made to obtain convergence of the support reactions, no solution startegy was found to accomplish this. When the solution was continued to the next load step, the displacement solution blew up.

At this point, it was decided to start a new analysis at the beginning of the second heatup-cooldown cycle for Layer 2. This approach is not rigorous in that the stresses are assumed to be zero at the beginning of the 2nd analysis, while in reality there is a non-zero stress field resulting from the Layer 1 heatup-cooldown cycle. However, because these stresses in Layer 1 are relieved during the second heat-up cycle as Layer 1 is effectively re-melted, this shortcoming does not appear to be particularly significant. Indeed, as can be seen from Figure V-3(b), Analysis 2 showed that an initial tip deflection developed, but could not be maintained as the temperature increased; and the plate settled back on the supports at about the same point as in Analysis 1. Error in the support reactions also occurred at this point of Analysis 2; on the next load step, however, balance between the weight of the plate and the support reactions was re-established.

From Figure V-3(a), it can be seen that Weld Layer 1 is effectively re-melted during the heatup for the deposit of Weld Layer 2 - achieving an average temperature of 1750°C at the point where Weld Layer 2 is introduced. As noted above, this results in the plate deflection returning to zero before Weld Layer 2 is deposited. Effectively, then, the analysis of Weld Layer 2 approaches the case of the deposit of an initial weld

layer whose size is the sum of Weld Layers 1 and 2. This phenomenon may explain whey the final predicted tip deflection is almost the same after the cooldown of Layer 2 as it was after the cooldown of Layer 1.

On cooldown, once sufficient strength has been achieved by the weld metal to provide the net moment necessary to deflect the plate, this net moment remains constant and the lateral deflection of the plate is controlled by the thermally-induced contraction. As a check on the NONSAP solutions, the moment that must exist at the inside support, to allow lift-off from the outside support, was calculated and compared to the net moment due to the axial stress distribution predicted by NONSAP at the inside support. The moment due to predicted stresses was approximately equal to the calculated required moment for all load steps where the plate is deflected, and was less than the required moment for all load steps where the plate is undeflected.

The plate behavior for deposit of Weld Layer 1 is straightforward. Until the finite element representing Layer 1 has cooled to a temperature low enough to achieve sufficient strength, the plate remains undeflected. At 760°C, the strength of the metal starts to increase dramatically (see Figure III-1), and

as the metal cools further, lift off from the outside support begins (Load Step 21). From this point (T=570°C), the temperature in and adjacent to Weld Layer 1 decreases uniformly until room temperature is reached. The thermal contraction of Weld Layer 1 and adjacent base plate controls the plate deflection. Because the weld layer lies above the neutral axis of the plate, the plate rotates such that the tip deflects upward. The final predicted tip deflection was 0.116 cm.

The plate behavior for deposit of Weld Layer 2 is more complex. From Figure V-3(b), Analysis 2 shows three regions during the heatup-cooldown cycle where the plate deflected. In Analysis 2, Weld Layer 1 is in place and is initially subjected to an increase in temperature. A uniform temperature increase of Weld Layer 1 would be expected to produce a negative tip deflection. However, the NONSAP analysis predicted a positive tip deflection during initial heatup. To explain this behavior, it is necessary to examine the temperature distribution in the element representing Weld Layer 1 and the adjacent element in the base plate.

The transient heat transfer analysis predicted temperatures at the locations of the nodes in the NONSAP model. The temperatures at the Gauss pts. in each element are a linear combination of these nodal temperatures. Figure V-4 shows the predicted

nodal temperatures and calculated temperatures at the Gauss pts. for the element representing Weld Layer 1 and the adjacent element in the base plate at load step 13 (where the early plate deflection peaks).

The nodal temperatures show a sharp thermal gradient from the weld centerline into the base plate. At the top of Weld Layer 1 and the adjacent element, the three nodal temperatures approximate the highly nonlinear thermal gradient. At the bottom of Weld Layer 1 and adjacent element, the two nodal temperatures can only represent a linear thermal gradient over the same distance into the plate.

The temperatures at the Gauss pts. in these two elements are calculated by linear interpolation from the nodal temperatures. Examination of the Gauss pt. temperatures indicates that the restrained thermal growth will be greater at the bottom of Weld Layer 1 and adjacent element than at the top. As a result, the plate is rotated such that the tip deflects upward.

Based on this evaluation of the plate behavior during early heatup, it is concluded that the positive plate deflection is not caused by physical considerations, but rather by the mathematical modelling approximations to the physical problem. The finite-element grid is inadequate to represent the actual thermal gradient over this short distance.

This deflection is transient; it is totally reversed when Weld Layer 1 loses the strength to support the plate in a deflected position, as the temperature increases above ≈600°C. Therefore, this early plate deflection does not contribute to the final permanent plate deflection after cooldown of Weld Layer 2.

The discussion above also applies to the plate deflection behavior predicted in Analysis 1, during the second heatup stage (dashed line in Figure V-3(b)). Here, the additional positive tip deflection is much less, because stresses approaching yield stress already exist after the cooldown of Layer 1. The thermally induced deflection behavior is not stress-free, since the temperature increase is far from uniform. The capability to carry additional stress is limited by the pre-existing stresses, which limits the amount of additional positive tip deflection.

Further along in Analysis 2, after settling back on the supports, the plate remains undeflected through the remaining heatup, the birth of Weld Layer 2, and the initial cooldown. Above 1500°C, the metal has negligible strength and cannot support a plate deflection. At load step 31, when the average temperature of Weld Layers 1 and 2 drops below 1500°C, the plate tip starts to deflect [see Figure V-3(b)]. Because the total thickness of the weld buildup is now doubled, the

moment needed to deflect the plate can develop at a much lower material strength level, and a correspondingly higher temperature. The transient plate deflection between load steps 31 and 39 appears to be caused by the different cooling rates for Weld Layers 1 and 2 [see Figure V-3(a)]. Initially, Weld Layer 2 cools at a faster rate and has a lower average temperature than Weld Layer 1, causing an upward tip deflection. Then, Weld Layer 1 cools at a faster rate than Weld Layer 2 and the average temperatures converge,causing a downward tip deflection. Finally, by load step 39, the cooling rates and average layer temperature equalize.

This transient deflection occurs in the weld layer temperature range 1500°C→760°C, before the major increase in material strength occurs (see Figure III-1). While the deflection is plausible, based on the weld layers temperature behavior, its physical significance is difficult to assess. Transient experimental data is unavailable for correlation; and it is conceivable that lack of restraint on the plate, coupled with approximations in the heat transfer and structural models, might produce an artificial effect in the high-temperature region of the solution. However, whether physical or not, this transient deflection does not contribute to the final plate deflection after complete cooldown.

The development of the final plate tip deflection begins with load step 40, when the weld layer temperatures drop below 760°C. From load steps 40 (T=670°C) to 44 (room temperature), the temperature decreases uniformly in and adjacent to Weld Layers 1 and 2. The pattern of deflection growth is very similar to that predicted in Analysis 1 for cooldown of Weld Layer 1. The final tip deflection after cooldown of Weld Layer 2 is 0.117 cm. upward, which is about 1% higher than the deflection after cooldown of Weld Layer 1.

It is difficult to evaluate the accuracy of the final tip deflection predictions from Analyses 1 and 2. Direct comparison to experimental data is not possible because there is no known correspondence between assumed Weld Layers 1 and 2 and the actual weld beads from the experiment. However, limited data was taken during the experiment, showing the average level of joint fill after beads 3, 4, 6, 8, and 9. Unfortunately, similar measurements were not taken after beads 1 and 2. Figure V-5 shows a plot of experimental tip deflection vs. height of joint fill, extrapolated back to zero deflection at zero fill height. Also shown are the NONSAP results for assumed Weld Layers 1 and 2. While the NONSAP results do not show an increase in tip deflection from Weld Layer 1 to Weld Layer 2, the predicted results are reasonably close to the extrapolated experimental curve.

Without additional heat transfer and thermo-structural analysis results for the remaining weld layers, the NONSAP results reported herein must be considered inconclusive. Future applications of the NONSAP approach should consider the complete fill of the weld joint, to better assess the accuracy of the analytical predictions.

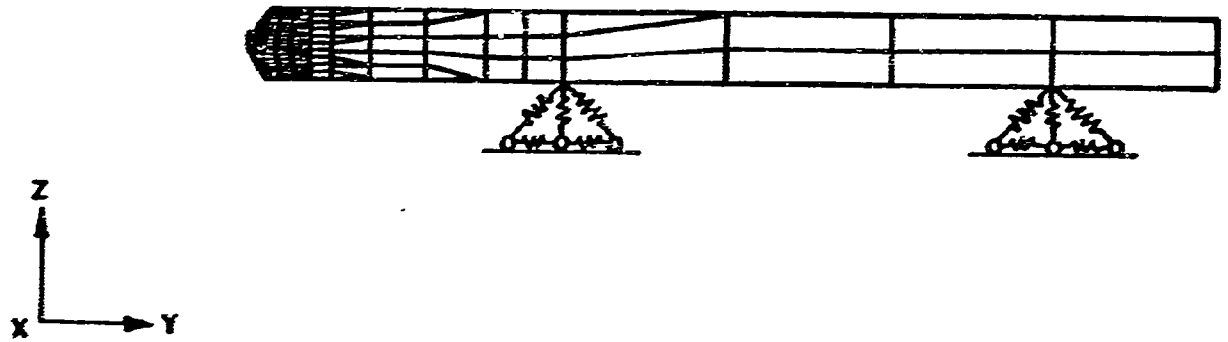

FIGURE V-1 NONSAP PLATE MODEL

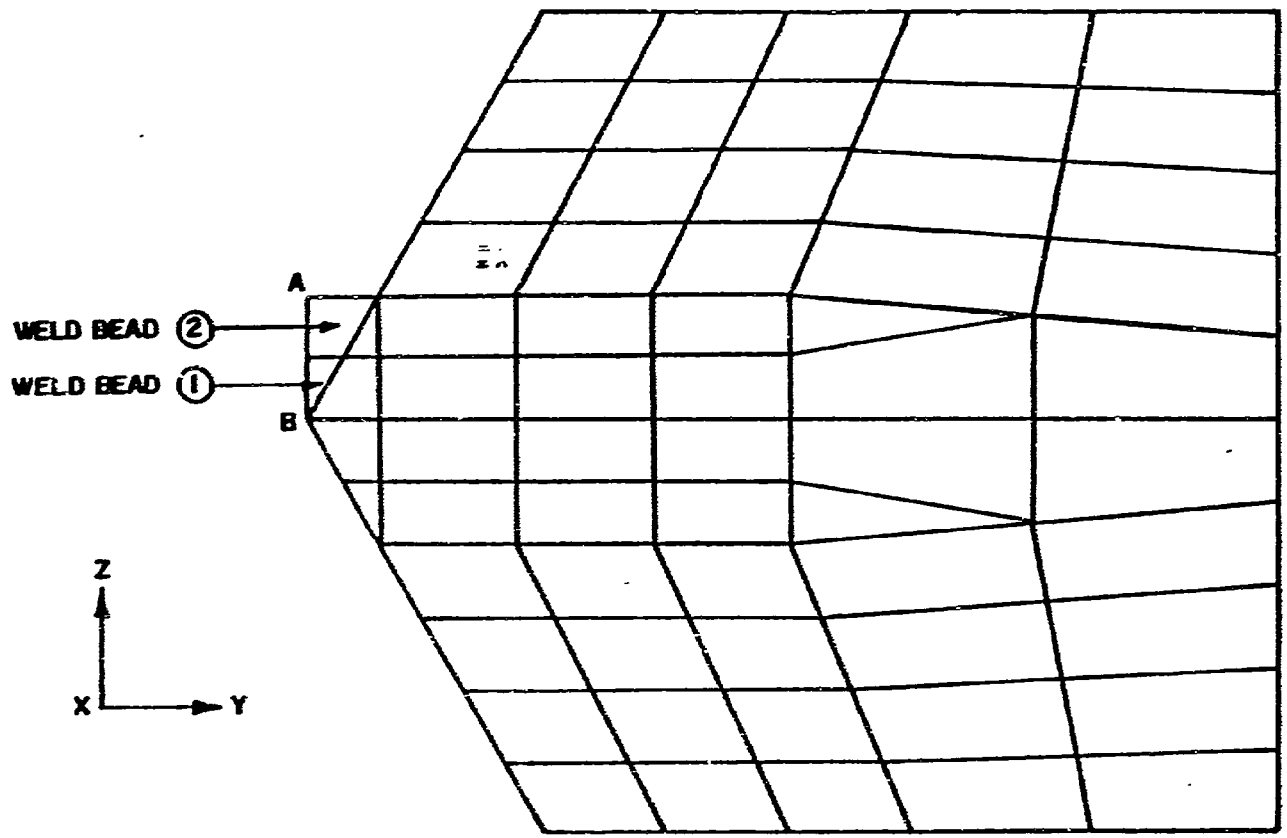

FIGURE V-2 WELD GROOVE REGION — NONSAP MODEL

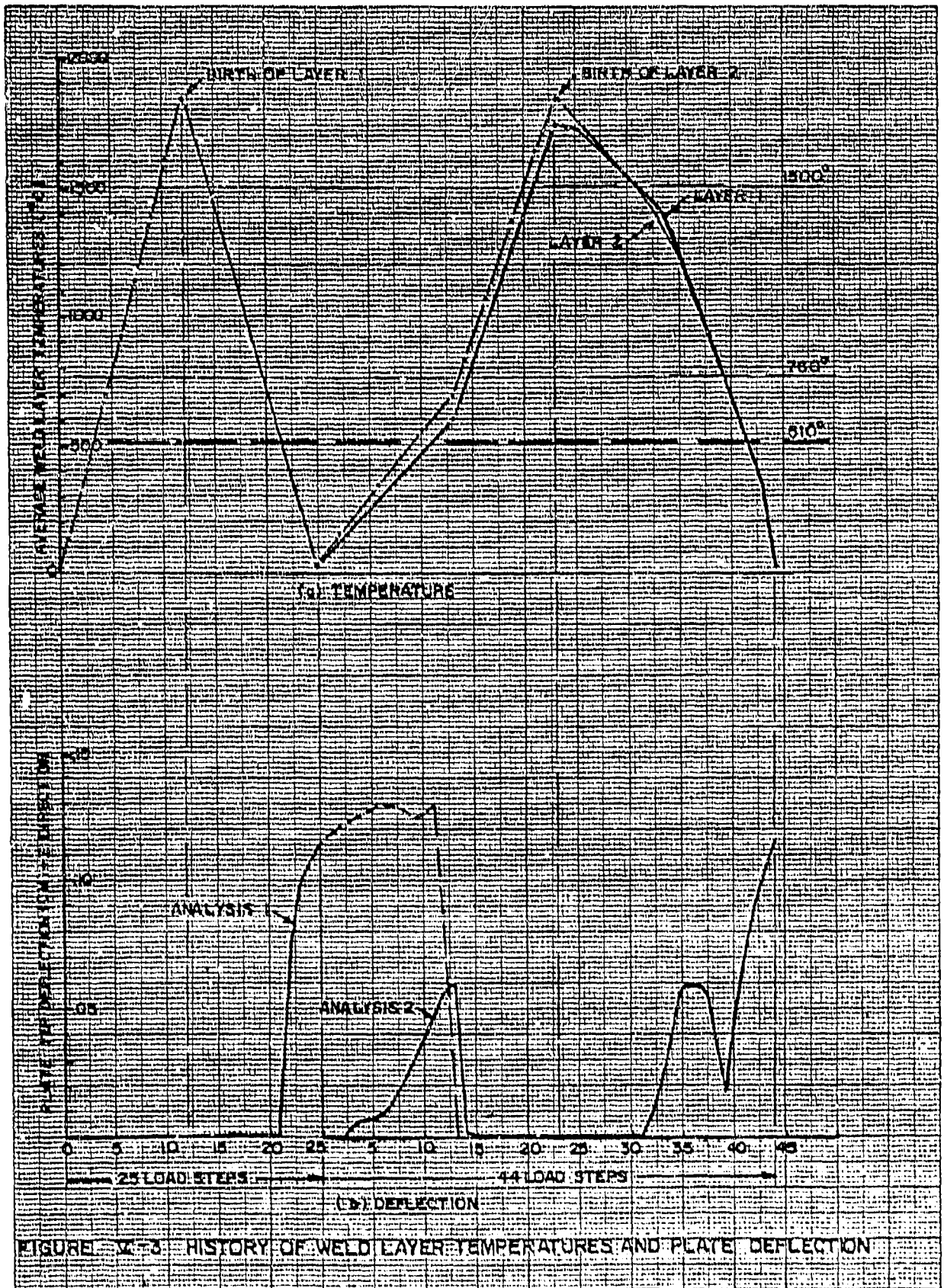

FIGURE V-3 HISTORY OF WELD LAYER TEMPERATURES AND PLATE DEFLECTION

EUGENE DIETZGEN CO.
MADE IN U.S.A.
NO. 340-H DIETZGEN GRAPH PAPER
MILLIMETER

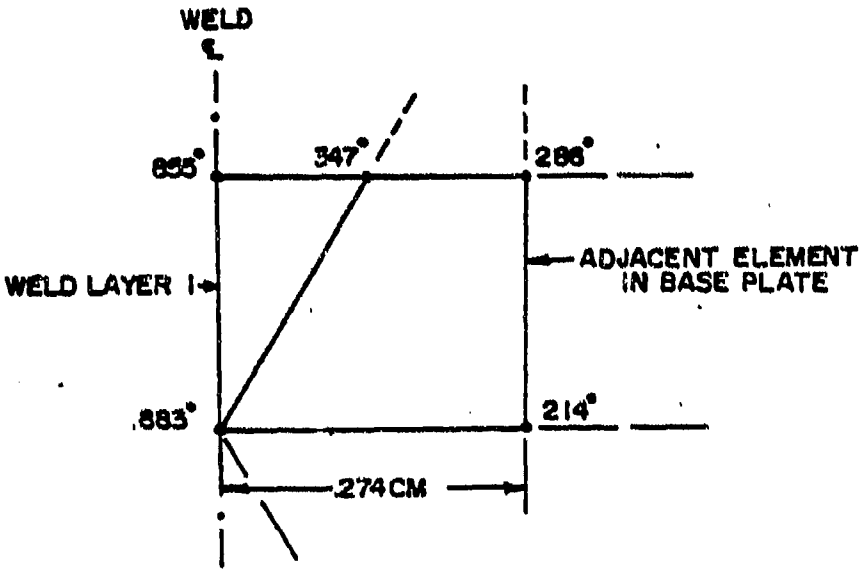

NODAL TEMPERATURES (°C)

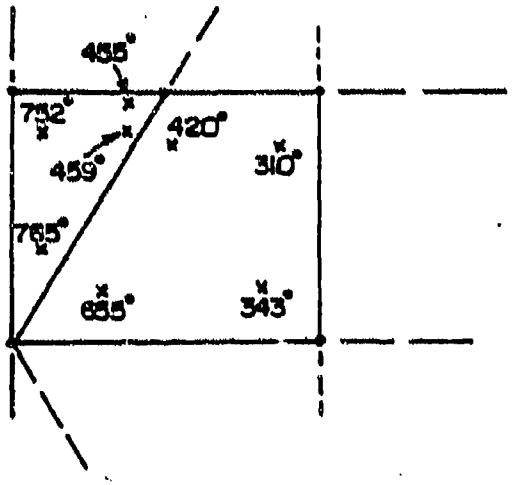

GAUSS POINT TEMPERATURES (°C)

FIGURE V-4 TEMPERATURES AT LOAD STEP 13, ANALYSIS 2 FOR WELD LAYER 1 AND ADJACENT BASE PLATE

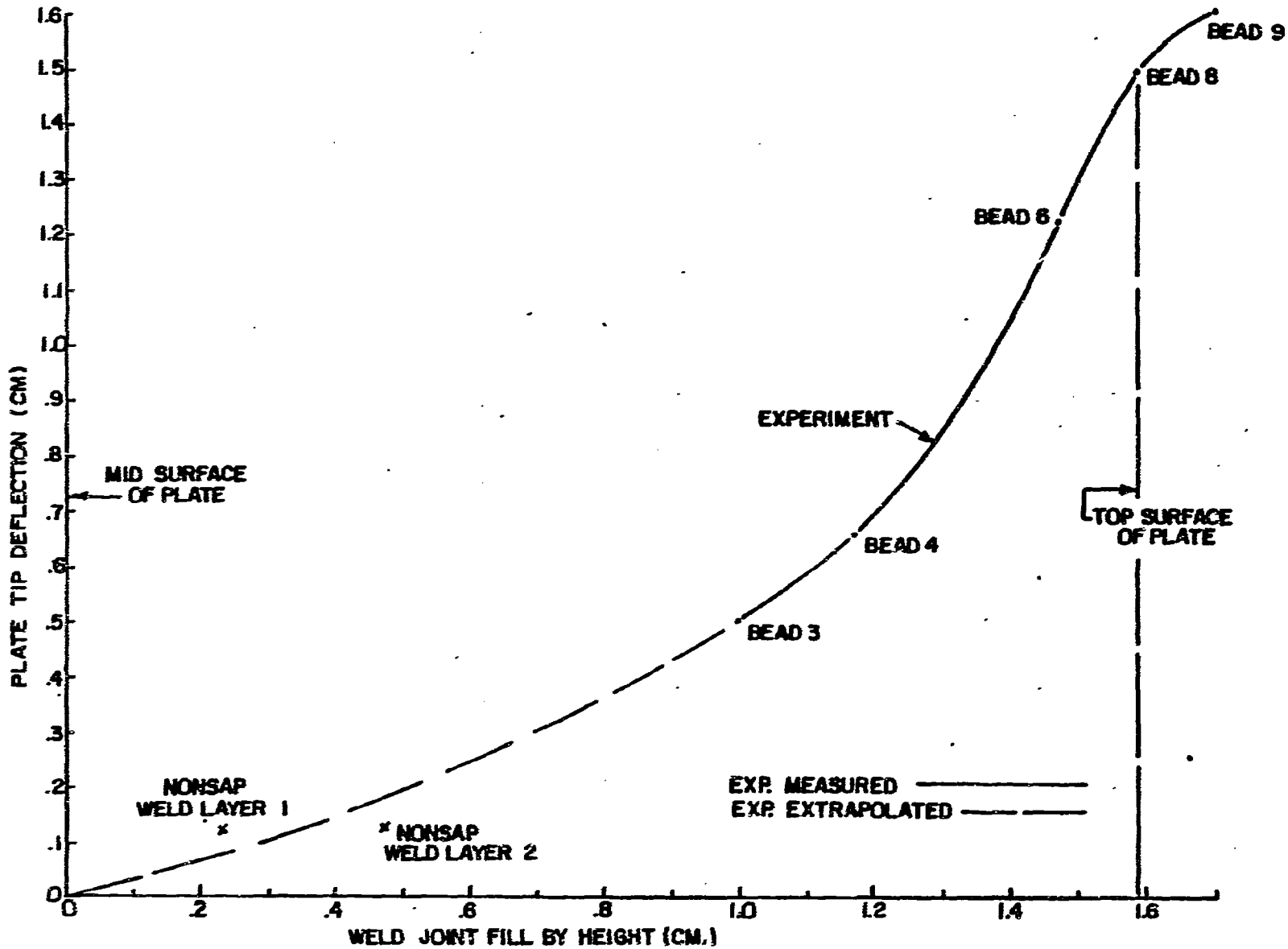

FIGURE V-5 NONSAP vs. EXPERIMENTAL DEFLECTIONS

VI. CONCLUSIONS AND RECOMMENDATIONS

VI-A. Shrinkage Force Analysis

The developments incorporated in this approach this year have brought about an overall improvement in the ability to predict distortion. A simple layer by layer approach without remelt effects provides a good initial solution for the distortion problem. Although the effects of remelt were not included in model 1 (layer model), results with later models indicated that remelt reduced the distortion in the early beads and became additive in the later beads. Applying this effect to the results for model 1 in Figure IV-8, it would improve the overall prediction of model 1. The bead approach used in models 2, 3, and 4 does provide a better approximation to the distortion. However, the information required to implement these models is extensive (bead profiles, remelt regions) and there remains a problem employing models of this type on shipyard problems.

For the unrestrained plate problem, reasonably accurate estimates of distortion were obtained without considering plasticity effects in the weld metal. This is not surprising since the structures being welded together offer minimal restraint to the shrinking weld metal. However, it is not clear why the predicted distortions were less than the measured distortions, since the assumption of elastic behavior of the weld metal would be expected to yield an upper bound analytical prediction for distortion.

The greatest discrepancy in the results was the inability of any of the models to predict the general increase in deflection that the experiment showed in going from Bead 4 to Bead 6 (Figure IV-16). No explanation can be found for this except that the bead representation and individual bead remelt geometry are still not sufficiently defined. Because of the required detailed bead description, application of models 2, 3 and 4 is somewhat limited. Methods which provide for predicting bead geometry and remelt will have to be developed before models such as these can be utilized fully. This appears to be feasible if the parameters of the welding process, such as rate and volume of deposit, average penetration etc., are known.

Based on the results of the SFM study the following conclusion can be drawn:

a) the simple layer model for unrestrained welds provide an adequate prediction of distortion for shipyard problems.

b) the effects of material property variation with temperature are important even in the simplest model of weld distortion.

c) plasticity effects were not significant in predicting weld distortion of unrestrained plates; however plasticity effects in restrained welds will be very important for accurate prediction of weld distortion.

d) the SFM retains several advantages (see Section IV-A) over more sophisticated methods, and is not restricted to a particular welding process or material.

e) useful results were obtained by SFM for this problem even with a coarse finite element subdivision of the weld region; however, the analysis of restrained welds with plasticity effects may require finer grids to insure sufficiently accurate calculation of the tangent stiffness in the weld region.

VI-B. NONSAP Analysis

Based on the NONSAP results obtained in this study, the permanent distortion appears to be controlled by behavior below 760°C, where the temperature decrease in and adjacent to the deposited weld metal is essentially uniform. Transient heat transfer analysis is important to define the extent of melting of solid metal when the current weld bead is being deposited. However, if this could be reasonably estimated based on past experience and experimental studies, the heat transfer analysis may not be essential for distortion prediction. Also, material property variations with temperature above 760°C - the region where they are most difficult to define - may not be essential to the analysis of distortion. These concepts are currently being investigated under an Electric Boat Division IRAD project to develop a second generation, shrinkage force method for predicting weld distortion.

As discussed in Section V, the NONSAP predictions of distortion obtained for assumed Weld Layers 1 and 2 are difficult to evaluate against the available experimental data; the results are considered inconclusive from a quantitative viewpoint. However, conceptually, the results are promising because the analytical model has demonstrated the ability to simulate fundamental behavior occurring during the welding process.

With improved input, refined modelling, and more comprehensive comparison with experimental data, the NONSAP approach may prove to be a valuable analytical tool for prediction of welding-induced structural behavior.

Considerable work remains to be done in both the heat transfer and structural analysis areas before detailed residual strasses can be accurately predicted. Based on the knowledge gained in the present study, the following conclusions are drawn concerning residual stress prediction:

a) performance of transient heat transfer and thermoplastic analyses for multi-pass welding problems is expensive, and for most shipyard applications it would be difficult to economically justify this approach for distortion prediction; for detailed residual stress analysis, this approach not only appears to be necessary but also will probably cost an order of magnitude more than a distortion analysis for comparable accuracy.

b) nonlinear heat transfer analysis and the correct determination of the transient temperature solutions is essential to welding residual stress analysis; more attention should be directed toward improvements in this area.

c) accurate representation of material property variations with temperatures up to melt appears necessary for residual stress analysis; additional work is needed in this area.

d) to accurately predict temperatures and stresses in the vicinity of the weld groove, the finite element discretization must be fine enough to pick up significant gradients over distances on the order of 10^{-1} cm.

VI-C. Recommendations

The following tasks are recommended for future investigations:

1) Analytically investigate the effects of varying key parameters in the heat transfer problem (heat deposit mechanism, heat dissipation to environment, material properties as functions of temperature) on the predicted transient temperature distributions that occur during girth welding of HY-80/130 steel cylinders.

2) Analytically predict transient temperature solution for girth welding of HY-130/HY-80 steel cylinders.

3) Compare analytical temperature predictions from 2) with the experimental results obtained by Professor Masubuchi at MIT.

4) Analytically predict transient thermoplastic distortions for the girth welding of HY-130/HY-80 cylinders and compare with experimental results from MIT.

5) Apply the Shrinkage Force Method (SFM) to predictions of thermomechanical distortions resulting from girth welding of HY-130/HY-80 cylinders and compare with experimental results from MIT.

6) Apply the Shrinkage Force Method to prediction of thermomechanical distortions resulting from girth welding of HY-80 submarine cylinders under shipyard conditions. Compare this data with measurements taken during actual weld construction.

7) Develop a detailed plan for determination of material property data for high strength steels such as HY-80.

VII. REFERENCES

1. Cacciatore, P. J., "Thermomechanical Finite Element Analysis of the Welding Process", Electric Boat Report No. P440-76-056, March, 1976.

2. Cacciatore, P. J., "Analytical Modeling of Heat Flow and Structural Distortion in Ship Structures Produced by Welding", Technical Report No. 1 for the Office of Naval Research under Contract No. N00014-76-C-0808, October, 1977.

3. Allik, H., and Cacciatore, P. J., "GENSAM USER'S MANUAL", Electric Boat Division Report No. P411-72-023, March, 1972.

4. Morante, R. J., "Development of Weld Distortion/Residual Stress Prediction Methods: Year-End Progress Report", Electric Boat Division Report No. ERR-EB78-005, April, 1978.

5. Gregory, A. H., and Romboni, A. H., "Weld Distortion Test of a Butt Welded HTS Flat Plate", Electric Boat Division Report No. P440-76-031, March, 1976.

6. Eldridge, E. A., and Deem, H. W., "Report on the Physical Properties of Metals and Alloys from Cryogenic to Elevated Temperatures", ASTM Special Technical Publication 296, 1961.

7. Simmons, E. F., and Cross, H. C., "Report on the Elevated-Temperature of Wrought Medium-Carbon Alloy Steels", ASTM Special Publication 199, 1957.

8. "Steels for Elevated Temperature Service", United States Steel Corporation, September, 1976.

UNCLASSIFIED

SECURITY CLASSIFICATION OF THIS PAGE (When Data Entered)

(14) **REPORT DOCUMENTATION PAGE**

READ INSTRUCTIONS BEFORE COMPLETING FORM

1. REPORT NUMBER: U443-79-087 (1)

2. GOVT ACCESSION NO.

3. RECIPIENT'S CATALOG NUMBER

4. TITLE (and Subtitle): Analytical Modeling of Structural Distortion in Ship Structures Produced by Welding. (9)

5. TYPE OF REPORT & PERIOD COVERED: Technical Report no. 2, July 1977-July 1978,

6. PERFORMING ORG. REPORT NUMBER

7. AUTHOR(s): P. J. Cacciatore, R. Morante (10)

8. CONTRACT OR GRANT NUMBER(s): N00014-76-C-0878 (15)

9. PERFORMING ORGANIZATION NAME AND ADDRESS: General Dynamics Corporation, Electric Boat Division, Groton, Connecticut

10. PROGRAM ELEMENT, PROJECT, TASK AREA & WORK UNIT NUMBERS: NR 031793

11. CONTROLLING OFFICE NAME AND ADDRESS: Office of Naval Research, Metallurgy Program, Arlington, Virginia (11)

12. REPORT DATE: December 1979

13. NUMBER OF PAGES: 89

14. MONITORING AGENCY NAME & ADDRESS (if different from Controlling Office): Office of Naval Research, Metallurgy Program, Arlington, Virginia (12) 92

15. SECURITY CLASS. (of this report): UNCLASSIFIED

15a. DECLASSIFICATION/DOWNGRADING SCHEDULE

16. DISTRIBUTION STATEMENT (of this Report)

17. DISTRIBUTION STATEMENT (of the abstract entered in Block 20, if different from Report)

18. SUPPLEMENTARY NOTES

19. KEY WORDS (Continue on reverse side if necessary and identify by block number): Welding, Simulation, Analysis, Heat Flow, Structural Distortion, Experimental Verification

20. ABSTRACT (Continue on reverse side if necessary and identify by block number)

This report describes the results of an investigation of the weld distortions produced in the welding of two simply supported plates. The analytical and experimental data for a multi-pass submerged arc weld of a balanced double-vee groove weld are presented. The analytical results were obtained using two mathematical approaches.

DD FORM 1 JAN 73 1473 EDITION OF 1 NOV 65 IS OBSOLETE S/N 0102-014-6601

UNCLASSIFIED

SECURITY CLASSIFICATION OF THIS PAGE (When Data Entered)

123 150

The first approach used was a quasi-linear approach identified as the Shrinkage Force Method. This method utilizes estimates of the cooldown forces in the weld region due to weld deposit and subsequent remelt, to predict distortion.

The second approach employs a full nonlinear thermoplastic analysis to predict distortions and residual stresses.

Several different mathematical models were employed in the study and the results obtained are compared with experimental data.